

# Beamspace Multidimensional ESPRIT Approaches for Simultaneous Localization and Communications

Fan Jiang, *Member, IEEE*, Fuxi Wen, *Senior Member, IEEE*, Yu Ge, *Student Member, IEEE*, Meifang Zhu, Henk Wymeersch, *Senior Member, IEEE*, Fredrik Tufvesson, *Fellow, IEEE*

**Abstract**—Modern wireless communication systems operating at high carrier frequencies are characterized by a high dimensionality of the underlying parameter space (including channel gains, angles, delays, and possibly Doppler shifts). Estimating these parameters is valuable for communication purposes, but also for localization and sensing, making channel estimation a critical component in any joint communication and localization or sensing application. The high dimensionality make it difficult to use search-based methods such as maximum likelihood. Search-free methods such as ESPRIT provide an attractive alternative, but require a complex decomposition step in both the tensor and matrix version of ESPRIT. To mitigate this, we propose, develop, and analyze a reduced complexity beamspace ESPRIT method. Complexity is reduced both by beamspace processing as well as low-complex implementation of the singular value decomposition. A novel perturbation analysis provides important insights for both channel estimation and localization performance. The proposed method is compared to the tensor ESPRIT method, in terms of channel estimation, communication, localization, and sensing performance, further validating the perturbation analysis.

## I. INTRODUCTION

Communication and localization are conventionally seen as competing for the same precious time-frequency resources, where reference signals used for localization take away resources used for communication. In that sense, one must trade off communication rate with localization accuracy [1], [2]. At the same time, it has been appreciated that location information is useful for communication [3]. For instance, since communication at high carrier frequencies is highly directional, location information can be an input in the design of precoders and combiners, illuminating only the dominant geometric propagation paths [4]. The explicit connection between communication and localization is via the channel estimation process. Typically, 5G mmWave channel estimation is based on a sparse and parametric representation of the channel, in which the parameters of the channel include the angles, distances, and gains [5]. These geometric parameters are also used for localization and mapping [6]. In turn, this means that

localization and communication are not competing, but can rather be integrated as a composed function. This naturally leads to simultaneous localization and communication (SLAC), i.e., a system where localization and communications go hand in hand. A challenge in channel estimation for 5G and beyond 5G is the large dimensionality [7]: a system with a moderate 1000 subcarriers and 64 antennas (e.g., an 8 by 8 planar array) at transmitter and receiver leads to a channel with 4 million parameters. Sparse estimation from such a large object is challenging and requires dedicated channel estimation methods.

Channel estimation methods can be roughly categorized as *search-based* and *search-free* methods. In the search-based methods we include techniques such as maximum likelihood [7], MUSIC [8], orthogonal matching pursuit [9], as well as other grid-based and sparsity-based methods [10]. These methods fundamentally require non-convex optimization over (at the minimum) the underlying parameter space, which can be prohibitively complex, especially since for both localization and communication, auto-pairing of the parameters across dimensions is required [11]. In contrast, search-free methods can provide a direct estimate of the channel parameters (i.e., tuples of delay and angles), often in the form of a closed-form expression [12]. Dominant in this category are the methods based on ESPRIT (for estimation of signal parameters via rotational invariance techniques) [13]–[15], which exploit the fundamental structure of the signal in its various domains. While ESPRIT is limited to certain types of signals, it turns out to be well-suited to typical waveforms and antenna arrangements in 5G and beyond 5G, including the use of OFDM and uniform planar arrays [16].

ESPRIT methods have been developed based on matrices of the observation (called multi-dimensional ESPRIT (MD-ESPRIT)) [11], as well as on tensors (called tensor ESPRIT) [15], [17] created from the observations. While the tensor version is arguably more natural, it suffers from high complexity due to the involved decomposition of the tensor. Furthermore, comparing with operation in element space, beamspace model offers a compromise between system performance and hardware complexity [18]. Tensor-based beamspace ESPRIT is proposed in [15], [19] for 3D mmWave channel estimation. An *R-D* search-free and general beamspace tensor-ESPRIT algorithm is proposed in [20]. Robustness of the method with respect to uncertainty in the number of sources, as well as the applicability for sources with partially distinct frequencies, are demonstrated in [21] for multidimensional harmonic retrieval. However, the performance is evaluated through numerical

Fan Jiang, Yu Ge, and Henk Wymeersch are with the Department of Electrical Engineering of Chalmers University of Technology, Gothenburg, Sweden. Email: {fan.jiang, yuge, henkw}@chalmers.se.

Fuxi Wen is with the School of Vehicle and Mobility, Tsinghua University, Beijing, China, Email: wenfuxi@tsinghua.edu.cn.

Meifang Zhu and Fredrik Tufvesson are with the Department of Electrical and Information Technology, Lund University, Lund, Sweden, Email: {meifang.zhu, fredrik.tufvesson}@eit.lth.se.

This work has been partly funded by the Vinnova 5GPOS project under grant 2019-03085, and by the Wallenberg AI, Autonomous Systems and Software Program (WASP) funded by the Knut and Alice Wallenberg Foundation.

simulations, perturbation analysis and positioning accuracy are not considered. In the case the observation is expressed as a large matrix or vector, MD-ESPRIT for angular frequency estimation is proposed in [11], a perturbation analysis on angular frequency estimation is also provided. However, it is an element-space based method, while a beamspace counterpart was not developed or analyzed.

In this paper, we consider a beamspace channel model with OFDM and URAs at both transmitter and receiver and propose an efficient and low-complex multidimensional beamspace ESPRIT method, based on which the user location and communication rate are estimated. The contributions of this paper are as follows:

- We develop a novel matrix-based multidimensional ESPRIT, operating in beamspace rather than channel space. To enable beamspace processing, we propose the use of modified selection matrices and show that arbitrary precoding and combining matrices can be used, provided they are full column-rank in each dimension. We also confirm that the auto-pairing property of element-space MD-ESPRIT holds in beamspace.
- We further propose a low-complexity implementation of the singular value decomposition (SVD) of the tall channel matrix in (beamspace) MD-ESPRIT, by using FFT/IFFT operations to obtain the signal subspace. We also demonstrate the low complexity through computational analysis and numerical simulations;
- We conduct a first-order perturbation analysis of the newly proposed MD-ESPRIT method, and evaluate both the analytical and numerical performance of the channel parameter and user location estimation. The results validate the closed-form analytical performance, especially in high signal-to-noise ratio (SNR) region;
- We evaluate the channel estimation and localization performance, as well as the effective achievable rate of the proposed method with both DFT and directional beams used in the system. The results reveal that our proposed beamspace MD-ESPRIT approaches achieve significant performance improvement compared to the methods in the literature;

The rest of the paper is organized as follows. In Section II, we introduce the system model including the multidimensional channel model, beamspace model, and beamspace observation model. We give an overview of the tensor-based ESPRIT approach for angular frequency estimation in Section III. After that, in section IV, we present the proposed matrix-based multidimensional beamspace ESPRIT approaches for SLAC, as well as the low-complexity implementations. Perturbation analysis is performed in Section V, where the closed-form analytical estimation performance of the proposed method is presented. Following that, we present the performance evaluation and discussions in Section VI. Finally, the conclusions are drawn in Section VII.

*Notations:* Vectors and matrices are denoted by bold lowercase and uppercase letters, respectively. The notations  $(\cdot)^*$ ,  $(\cdot)^T$ ,  $(\cdot)^H$ ,  $(\cdot)^{-1}$ , and  $(\cdot)^\dagger$ , are reserved for the conjugate, transpose, conjugate transpose, inverse, and Moore-Penrose pseudoinverse operations. The mathematical expectation is

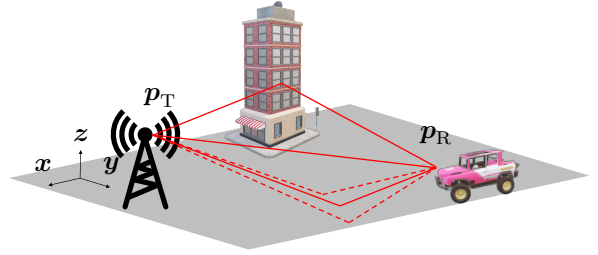


Fig. 1: 3D localization and communications with multi-path propagation: vehicular user with unknown location using LOS/NLOS signals from base station with known position to localize itself; the vehicular user also expecting to know the effective achievable rate in communications.

denoted by  $E\{\cdot\}$ . The notation  $\text{Diag}(\mathbf{a})$  is to form a diagonal matrix with  $\mathbf{a}$  being the diagonal elements. The operations  $\otimes$  and  $\odot$  denote the Kronecker and Khatri-Rao products, respectively. The outer product is denoted by  $\circ$ .  $\delta(\cdot)$  is the delta Dirac function. The notations  $\Re\{\cdot\}$  and  $\Im\{\cdot\}$  denote the operations to obtain the real and imaginary components, respectively.

## II. SYSTEM MODEL

### A. Multidimensional Channel Model

We consider a 3-dimensional (3D) scenario for vehicular localization and communications as shown in Fig. 1. The base station and the vehicular terminal are located at  $p_T$  and  $p_R$ , respectively. Both the transmitter and the receiver are equipped with uniform rectangular arrays (URA) in  $y-z$  plane consisting of  $M_T = M_1 \times M_2$  and  $M_R = M_3 \times M_4$  antenna elements, respectively. The antenna spacing is  $\Delta d = \lambda/2$ , where  $\lambda$  is the wavelength. We consider a multi-path propagation scenario, where both line-of-sight (LOS) and non LOS (NLOS) paths are present in the system. The NLOS paths can be either reflection paths or diffuse multi-path depending on the smoothness of the objects in the environment. Each propagation path will be associated with AODs  $\phi_l = [\phi_{az}^l, \phi_{el}^l]^T$ , AOAs  $\theta_l = [\theta_{az}^l, \theta_{el}^l]^T$ , the propagation delay  $\tau_l$ , and the complex gain  $\gamma_l$ . We use  $\phi_{az}^l$  and  $\phi_{el}^l$  to denote the azimuth angle in the  $x-y$  plane and the elevation angle for AODs, respectively, whereas  $\theta_{az}^l$  and  $\theta_{el}^l$  to denote the azimuth angle in the  $x-y$  plane and the elevation angle for the AOAs, respectively. The geometric relationship between the positions and the channel parameters can be found in [6], [22].

We assume OFDM transmission with  $M_5$  subcarriers under narrow-band, far-field conditions, and possibly precoding and combining. To this end, we introduce  $\mathbf{T}_n^H = [t_{n,1}, t_{n,2}, \dots, t_{n,M_n}] \in \mathbb{C}^{N_n \times M_n}$  as a transformation matrix, allowing us to write a precoding matrix  $\mathbf{F} = (\mathbf{T}_1 \otimes \mathbf{T}_2)^* \in \mathbb{C}^{M_1 M_2 \times N_1 N_2}$  at transmitter side and a combining matrix  $\mathbf{W} = \mathbf{T}_3 \otimes \mathbf{T}_4 \in \mathbb{C}^{M_3 M_4 \times N_3 N_4}$  at receiver side. We assume no precoding is applied to the frequency domain, i.e.,  $\mathbf{T}_5 = \mathbf{I}_{M_5}$ . As a result, the beamspace channel matrix over the  $m_5$ -th subcarrier,  $\mathbf{H}_{m_5}^{(b)} \in \mathbb{C}^{N_3 N_4 \times N_1 N_2}$  will be given by

$$\mathbf{H}_{m_5}^{(b)} = \sum_{l=1}^L \gamma_l e^{-j2\pi(m_5-1)\Delta f \tau_l} \mathbf{W}^H \mathbf{a}_R(\theta_l) \mathbf{a}_T^T(\phi_l) \mathbf{F}, \quad (1)$$

where  $\Delta f$  is the subcarrier spacing,  $L$  denotes the number of propagation paths,  $l = 1$  is the LOS path and the rest ( $l > 1$ ) are NLOS paths. The steering vector corresponding to the  $l$ -th propagation path at transmitter side is given by [22]

$$\mathbf{a}_T(\phi_l) = \mathbf{a}^{(M_1)}(\omega_{l,1}) \otimes \mathbf{a}^{(M_2)}(\omega_{l,2}), \quad (2)$$

where  $\omega_{l,1} = \pi \sin(\phi_{az}^l) \sin(\phi_{el}^l)$ ,  $\omega_{l,2} = \pi \cos(\phi_{el}^l)$ ,  $\otimes$  is the Kronecker product, and  $\mathbf{a}^{(M)}(\omega)$  is a Vandermonde-structured vector defined as

$$\mathbf{a}^{(M)}(\omega) = [1, \exp(j\omega), \dots, \exp(j(M-1)\omega)]^T.$$

Similarly, the steering vector at the receiver side is given by

$$\mathbf{a}_R(\theta_l) = \mathbf{a}^{(M_3)}(\omega_{l,3}) \otimes \mathbf{a}^{(M_4)}(\omega_{l,4}), \quad (3)$$

where  $\omega_{l,3} = \pi \sin(\theta_{az}^l) \sin(\theta_{el}^l)$ ,  $\omega_{l,4} = \pi \cos(\theta_{el}^l)$ .

It will be convenient to introduce  $\mathbf{B}_n^{(N_n)} \in \mathbb{C}^{N_n \times L}$  as

$$\mathbf{B}_n^{(N_n)} = \mathbf{T}_n^H \mathbf{A}_n^{(M_n)}, \quad (4)$$

where  $\mathbf{A}_n^{(M_n)} \in \mathbb{C}^{M_n \times L}$  is the Vandermonde matrix of the mode in the  $n$ -th dimension, given by  $\mathbf{A}_n^{(M_n)} = [\mathbf{a}^{(M_n)}(\omega_{1,n}), \mathbf{a}^{(M_n)}(\omega_{2,n}), \dots, \mathbf{a}^{(M_n)}(\omega_{L,n})]$ .

### B. BeamSpace Observation Model

We consider a scenario where the channel coefficients remain static for a period of  $N_c$  OFDM blocks. The first  $N_P$  OFDM blocks will be used for pilots transmission, and the rest  $N_D = N_C - N_P$  OFDM blocks will be used for data transmission. We suppose the transmitter and receiver are equipped with  $N_1 \times N_2$  and  $N_3 \times N_4$  RF chains, respectively.<sup>1</sup> During the pilot transmission stage, the pilot matrix  $\mathbf{S}_{m_5} \in \mathbb{C}^{N_1 N_2 \times N_P}$  is transmitted over the  $m_5$ -th subcarrier where  $\mathbf{S}_{m_5} \mathbf{S}_{m_5}^H = N_P E_s \mathbf{I}_{N_1 N_2}$ , where we assume  $N_P \geq N_1 N_2$  and the power of the pilot symbols are normalized to  $E_s$ . With the transmit pilots, the corresponding beamSpace received symbols over the  $m_5$ -th subcarrier will be

$$\mathbf{Y}_{m_5} = \mathbf{H}_{m_5}^{(b)} \mathbf{S}_{m_5} + \mathbf{Z}_{m_5}, \quad (5)$$

where  $\mathbf{Y}_{m_5} \in \mathbb{C}^{N_3 N_4 \times N_P}$ . The matrix  $\mathbf{Z}_{m_5} \in \mathbb{C}^{N_3 N_4 \times N_P}$  is the beamSpace noise component over the  $m_5$ -th subcarrier, with each entry modelled as independent and identically distributed (iid) zero mean complex Gaussian random variable. The variance of each entry is  $N_0$ . From (5), we obtain the beamSpace channel estimate  $\hat{\mathbf{H}}_{m_5}^{(b)} \in \mathbb{C}^{N_3 N_4 \times N_1 N_2}$  given by

$$\hat{\mathbf{H}}_{m_5}^{(b)} = \frac{\mathbf{Y}_{m_5} \mathbf{S}_{m_5}^H}{N_P E_s} = \mathbf{H}_{m_5}^{(b)} + \Delta \mathbf{H}_{m_5}^{(b)}, \quad (6)$$

where  $\Delta \mathbf{H}_{m_5}^{(b)} \in \mathbb{C}^{N_3 N_4 \times N_1 N_2}$  is the channel estimation error matrix, with each entry  $\Delta h_{n_1, n_2, n_3, n_4, m_5}$  modelled as iid zero mean complex Gaussian variable with variance  $N_0 / (N_P E_s)$ .

<sup>1</sup>The beamSpace observation in can also be obtained with an arbitrary number of RF chains at transmitter and receivers. Let  $N_T$  and  $N_R$  denote the number of RF chains at transmitter and receiver, respectively. Generally, we can use  $N_1 N_2 N_3 N_4 / N_R$  transmission to obtain (6).

### C. Goals

Collecting the beamSpace channel estimates  $\hat{\mathbf{H}}_{m_5}^{(b)}$  over all subcarriers, our objectives are to estimate the angular frequencies  $[\omega_{l,1}, \dots, \omega_{l,5}]^T$  and  $\gamma_l$  per path, as well as their uncertainties, and compute the estimates of the channel parameters  $\boldsymbol{\eta}_l = [\phi_l^T, \theta_l^T, \tau_l, \gamma_l]^T$ , based on the one-to-one mapping between the angular frequencies and the spatial channel parameters (TOAs, AOA, AODs).

Our second objective is the SLAC analysis, which involves computation of the user location and associated uncertainty, and assessment of the communication performance with beamSpace observations. We use off-the-shelf solutions for localization and rate prediction, as shown below. We note that both the localization and communication performance are affected by the channel estimation.

1) *Location Estimation*: We employ the method from [22], [23] for localization, due to its simple closed-form expression. Specifically, we define the unit vectors

$$\begin{aligned} \mathbf{f}_{T,l} &= [\cos(\hat{\phi}_{az}^l) \sin(\hat{\phi}_{el}^l), \sin(\hat{\phi}_{az}^l) \sin(\hat{\phi}_{el}^l), \cos(\hat{\phi}_{el}^l)]^T, \\ \mathbf{f}_{R,l} &= [\cos(\hat{\theta}_{az}^l) \sin(\hat{\theta}_{el}^l), \sin(\hat{\theta}_{az}^l) \sin(\hat{\theta}_{el}^l), \cos(\hat{\theta}_{el}^l)]^T, \end{aligned}$$

as the direction vectors for the  $l$ -th AODs and AOAs, respectively. For each propagation path, we define  $\boldsymbol{\mu}_l = c\hat{\tau}_l(\mathbf{f}_{T,l} + \mathbf{f}_{R,l})$  and  $\boldsymbol{\delta}_l = \mathbf{p}_T - c\hat{\tau}_l \mathbf{f}_{R,l}$ . The weighted least-squares solution of  $\mathbf{p}_R$  is given by

$$\hat{\mathbf{p}}_R = \left( \sum_{l=1}^L \mathbf{C}_l \right)^{-1} \sum_{l=1}^L \mathbf{C}_l \boldsymbol{\delta}_l, \quad (7)$$

where  $\mathbf{C}_l = \iota_l (\mathbf{I} - \boldsymbol{\mu}_l \boldsymbol{\mu}_l^T / \|\boldsymbol{\mu}_l\|^2)$  and  $\{\iota_l\}_{l=1}^L \geq 0$  is the weight dependent on the SNR.

2) *Communication Rate Prediction*: We follow the method in [24] to compute the effective achievable rate; we first derive the signal-to-interference-plus-noise ratio (SINR), and then compute the sum-rate. After channel estimation, under single-stream transmission, we determine (possibly subcarrier dependent) optimal precoders  $\mathbf{f}_{\text{com}}$  and combiners  $\mathbf{w}_{\text{com}}$ , leading to the effective channel on subcarrier  $m_5$

$$h_{m_5} = \underbrace{\mathbf{w}_{\text{com}}^H \hat{\mathbf{H}}_{m_5} \mathbf{f}_{\text{com}}}_U - \underbrace{\mathbf{w}_{\text{com}}^H \Delta \mathbf{H}_{m_5} \mathbf{f}_{\text{com}}}_I, \quad (8)$$

where  $\hat{\mathbf{H}}_{m_5} = \sum_{l=1}^L \hat{\gamma}_l e^{-j2\pi(m_5-1)\Delta f \tau_l} \mathbf{a}_R(\hat{\boldsymbol{\theta}}_l) \mathbf{a}_T^T(\hat{\boldsymbol{\phi}}_l)$ , and  $\Delta \mathbf{H}_{m_5}$  is the estimation error, due to the observation noise and the channel estimation routine. We can compute a SINR over the  $m_5$ -th subcarrier,  $\eta_{m_5} = |U|^2 / (N_0 + E\{|I|^2\})$ , leading to an effective achievable rate

$$R = \frac{N_C - N_P}{M_5 N_C} \sum_{m_5=1}^{M_5} \log_2(1 + \eta_{m_5}). \quad (9)$$

## III. TENSOR-BASED BEAMSPACE ESPRIT

The high-dimensional beamSpace channel can be naturally represented by the tensor  $\mathcal{H}^{(b)} \in \mathbb{C}^{N_1 \times N_2 \times \dots \times N_5}$ , with canonical polyadic model

$$\mathcal{H}^{(b)} = \sum_{l=1}^L \gamma_l \mathbf{b}^{(N_1)}(\omega_{l,1}) \circ \dots \circ \mathbf{b}^{(N_5)}(\omega_{l,5}), \quad (10)$$

---

**Algorithm 1** BeamSpace Tensor ESPRIT Approach [21]
 

---

**Input:** Noisy beamSpace observation  $\hat{\mathcal{H}}^{(b)}$ ;

**Output:** Channel parameter estimates:  $\phi_{\text{el}}^l, \phi_{\text{az}}^l, \theta_{\text{el}}^l, \theta_{\text{az}}^l$ , and  $\tau_l$ , for  $l = 1, 2, \dots, L$ .

- 1: Apply CP decomposition on  $\hat{\mathcal{H}}^{(b)}$  to obtain  $\mathbf{U}_n$  (11);
  - 2: Determine  $\mathbf{F}_n$  and  $\mathbf{Q}_n$  from Proposition 1;
  - 3: Obtain  $\mathbf{L}_{n,1} = \mathbf{Q}_n$  and  $\mathbf{L}_{n,2} = \mathbf{Q}_n \mathbf{F}_n^{\text{H}}$ ;
  - 4: Obtain  $\mathbf{\Gamma}_n = (\mathbf{L}_{n,2} \mathbf{U}_n)^\dagger (\mathbf{L}_{n,1} \mathbf{U}_n)$
  - 5: Perform the eigenvalue decomposition of  $\mathbf{\Gamma}_n$  to obtain the matrix of complex eigenvalues  $\mathbf{D}_n = \text{Diag}([d_{n,1}, d_{n,2}, \dots, d_{n,L}]^{\text{T}})$ , and the angular frequencies in the  $n$ -th mode are given by  $\hat{\omega}_{l,n} = \Im\{\ln(\hat{\Phi}_{l,n})\}$  for  $l = 1, 2, \dots, L$ .
  - 6: Obtain the channel parameter estimates [6], [22].
- 

where  $\circ$  denotes the outer product and  $\mathbf{b}^{(N_n)}(\omega_{l,n}) = \mathbf{T}_n^{\text{H}} \mathbf{a}^{(M_n)}(\omega_{l,n})$ , and  $N_5 = M_5$ . To estimate the angular frequencies  $\omega_{l,n}$  from a noisy version of  $\mathcal{H}^{(b)}$ , we briefly recap the beamSpace tensor ESPRIT method from [21].

#### A. Tensor Decomposition

CANDECOMP/PARAFAC (CP) and Tucker are two widely used tensor decomposition approaches [25]. By apply CP decomposition on noisy measurement  $\hat{\mathcal{H}}^{(b)}$  in (10), we obtain  $\hat{\mathcal{H}}^{(b)} \approx \sum_{l=1}^L \lambda_l \mathbf{u}_{l,1} \circ \mathbf{u}_{l,2} \circ \mathbf{u}_{l,3} \circ \mathbf{u}_{l,4} \circ \mathbf{u}_{l,5}$ , where  $\lambda_l, l = 1, 2, \dots, L$ , are the dominant eigenvalues. The eigenvectors in the  $n$ -th dimension can be described as

$$\mathbf{U}_n = [\mathbf{u}_{1,n} \quad \mathbf{u}_{2,n} \quad \dots \quad \mathbf{u}_{L,n}] \in \mathbb{C}^{N_n \times L}, n = 1, 2, \dots, 5. \quad (11)$$

Since  $\mathbf{B}_n^{(N_n)}$  is also spanned by the signal subspace, there exists a non-singular matrix  $\mathbf{E}_n \in \mathbb{C}^{L \times L}$ , satisfying  $\mathbf{B}_n^{(N_n)} = \mathbf{U}_n \mathbf{E}_n$ .

#### B. Tensor-based ESPRIT for Angular Frequency Estimation

We first define the following selection matrices  $\mathbf{J}_{n,1} = [\mathbf{I}_{N_n-1}, \mathbf{0}_{(N_n-1) \times 1}]$  and  $\mathbf{J}_{n,2} = [\mathbf{0}_{(N_n-1) \times 1}, \mathbf{I}_{N_n-1}]$  and let  $\mathbf{\Phi}_n = \text{Diag}\{[\Phi_{1,n}, \Phi_{2,n}, \dots, \Phi_{L,n}]^{\text{T}}\}$  with  $\Phi_{l,n} = \exp(j\omega_{l,n})$ . ESPRIT relies on the so-called shift invariance property to perform the angular frequency estimation, meaning that  $\mathbf{J}_{n,1} \mathbf{A}_n^{(N_n)} \mathbf{\Phi}_n = \mathbf{J}_{n,2} \mathbf{A}_n^{(N_n)}$ . In beamSpace, generally with the transformation matrix  $\mathbf{T}_n$ ,  $\mathbf{J}_{n,1} \mathbf{B}_n^{(N_n)} \mathbf{\Phi}_n \neq \mathbf{J}_{n,2} \mathbf{B}_n^{(N_n)}$ . However, if  $\mathbf{T}_n$  itself has a shift invariance structure, the following proposition shows that the lost shift invariance structure can be restored.

**Proposition 1.** Assume that  $\mathbf{T}_n \in \mathbb{C}^{M_n \times N_n}$  has the shift invariance structure  $\mathbf{J}_{n,1} \mathbf{T}_n = \mathbf{J}_{n,2} \mathbf{T}_n \mathbf{F}_n$  where  $\mathbf{F}_n \in \mathbb{C}^{N_n \times N_n}$  is a non-singular matrix. If there exists a matrix  $\mathbf{Q}_n \in \mathbb{C}^{N_n \times N_n}$ , such that  $\mathbf{Q}_n \mathbf{t}_{n,M_n} = \mathbf{0}_{N_n \times 1}$  and  $\mathbf{Q}_n \mathbf{F}_n^{\text{H}} \mathbf{t}_{n,1} = \mathbf{0}_{N_n \times 1}$ , then  $\mathbf{Q}_n \mathbf{B}_n^{(N_n)} \mathbf{\Phi}_n = \mathbf{Q}_n \mathbf{F}_n^{\text{H}} \mathbf{B}_n^{(N_n)}$ .

*Proof.* The proof can be found in [14], [20].  $\square$

Proposition 1 indicates that we can restore the shift invariance properties by forming the matrix  $\mathbf{Q}_n$  as a projection

matrix corresponding to the orthogonal subspace spanned by  $\mathbf{t}_{n,M_n}, \mathbf{F}_n^{\text{H}} \mathbf{t}_{n,1}$ . In particular, let  $\mathbf{p}_{n,1}$  and  $\mathbf{p}_{n,2}$  be the orthogonal column vectors for this subspace, then  $\mathbf{Q}_n$  can be obtained as  $\mathbf{Q}_n = \mathbf{I}_{N_n} - \sum_{k=1}^2 \mathbf{p}_{n,k} \mathbf{p}_{n,k}^{\text{H}}$ . When a  $\mathbf{Q}_n$  is determined, the shift-invariance property in the  $n$ -th mode can be restored with the following modified selection matrices

$$\mathbf{L}_{n,1} = \mathbf{Q}_n, \quad (12)$$

$$\mathbf{L}_{n,2} = \mathbf{Q}_n \mathbf{F}_n^{\text{H}}. \quad (13)$$

When the shift invariance structure does not hold for  $\mathbf{T}_n$ , i.e.,  $\mathbf{J}_{n,1} \mathbf{T}_n \neq \mathbf{J}_{n,2} \mathbf{T}_n \mathbf{F}_n$ , we can find an approximate non-singular  $N_n \times N_n$  matrix  $\tilde{\mathbf{F}}_n$ , such that  $\mathbf{J}_{n,1} \mathbf{T}_n \approx \mathbf{J}_{n,2} \mathbf{T}_n \tilde{\mathbf{F}}_n$ . The least-square solution is given as  $\tilde{\mathbf{F}}_n = (\mathbf{J}_{n,2} \mathbf{T}_n)^\dagger \mathbf{J}_{n,1} \mathbf{T}_n$  from which  $\mathbf{Q}_n$  can be obtained as before.

Finally, the beamSpace Tensor ESPRIT method [21] is summarized in Algorithm 1.

## IV. MATRIX-BASED BEAMSPACE ESPRIT

As an alternative to the tensor approach, we present a novel matrix-based approach for beamSpace ESPRIT. By vectorizing the beamSpace tensor  $\mathcal{H}^{(b)}$ , we arrive at

$$\begin{aligned} \mathbf{h}^{(b)} &= \text{vec}_{\text{r}}\{\mathcal{H}^{(b)}\} = [h_{1,1,1,1,1,1}^{(b)}, h_{1,1,1,1,1,2}^{(b)}, \dots, h_{1,1,1,1,1,M_5}^{(b)}, \\ &\quad h_{1,1,1,2,1,1}^{(b)}, \dots, h_{N_1, N_2, N_3, N_4, M_5}^{(b)}]^{\text{T}}, \\ &= (\mathbf{B}_1^{(N_1)} \odot \mathbf{B}_2^{(N_2)} \odot \dots \odot \mathbf{B}_5^{(N_5)}) \boldsymbol{\gamma}, \end{aligned} \quad (14)$$

where  $\odot$  is the Khatri-Rao product,  $\boldsymbol{\gamma} = [\gamma_1, \gamma_2, \dots, \gamma_L]^{\text{T}}$ .

The proposed method has three parts: spatial smoothing for improved resolution, a novel low-complexity SVD of the channel matrix, and auto-paired angular frequency estimation.

#### A. Spatial Smoothing

Considering  $\mathbf{T}_5 = \mathbf{I}_{M_5}$ , we can apply spatial smoothing in the frequency domain. Specifically, we define the selection matrices

$$\begin{aligned} \mathbf{J}_{\ell_5} &= [\mathbf{0}_{K_5 \times (\ell_5-1)}, \mathbf{I}_{K_5}, \mathbf{0}_{K_5 \times (L_5-\ell_5)}], \\ \mathbf{J}_{N_1, N_2, N_3, N_4, \ell_5} &= \mathbf{I}_{N_1} \otimes \mathbf{I}_{N_2} \otimes \mathbf{I}_{N_3} \otimes \mathbf{I}_{N_4} \otimes \mathbf{J}_{\ell_5}, \end{aligned}$$

where  $L_5 + K_5 = M_5 + 1$ . We then construct a matrix  $\mathbf{H} \in \mathbb{C}^{N_1 N_2 N_3 N_4 K_5 \times L_5}$  as

$$\begin{aligned} \mathbf{H} = \mathcal{S}(\mathbf{h}^{(b)}) &= [\mathbf{J}_{N_1, N_2, N_3, N_4, 1} \mathbf{h}^{(b)}, \\ &\quad \mathbf{J}_{N_1, N_2, N_3, N_4, 2} \mathbf{h}^{(b)}, \dots, \mathbf{J}_{N_1, N_2, N_3, N_4, L_5} \mathbf{h}^{(b)}], \end{aligned} \quad (15)$$

where we use  $\mathcal{S}(\cdot)$  to denote the smoothing operation over the frequency domain.

#### B. Signal Subspace and Shift Invariance Properties

From Appendix A, we can see that  $\mathbf{H}$  can be factorized as

$$\mathbf{H} = \mathbf{P} \text{Diag}(\boldsymbol{\gamma}) \mathbf{G}^{\text{T}}, \quad (16)$$

where  $\mathbf{P} \in \mathbb{C}^{N_1 N_2 N_3 N_4 K_5 \times L}$  and  $\mathbf{G} \in \mathbb{C}^{L_5 \times L}$ , given by

$$\mathbf{P} = \mathbf{B}_1^{(N_1)} \odot \dots \odot \mathbf{B}_4^{(N_4)} \odot \mathbf{A}_5^{(K_5)}, \quad (17)$$

$$\mathbf{G} = \mathbf{A}_5^{(L_5)}. \quad (18)$$

The following proposition shows that the shift invariance properties can be restored with the matrix formulation.

**Proposition 2.** Assume that  $\mathbf{T}_n$ ,  $n = 1, 2, 3, 4$ , has the shift invariance structure, and  $\mathbf{P}$  is given in (17), we then have

$$\check{\mathbf{J}}_{n,1} \mathbf{P} \check{\Phi}_n = \check{\mathbf{J}}_{n,2} \mathbf{P}, \quad (19)$$

where  $\check{\mathbf{J}}_{n,i}$ ,  $n = 1, 2, \dots, N$ , and  $i = 1, 2$ , is defined as follows:

$$\check{\mathbf{J}}_{n,i} = \begin{cases} \mathbf{I}_{N_1} \otimes \dots \otimes \mathbf{L}_{n,i} \otimes \dots \otimes \mathbf{I}_{N_4} \otimes \mathbf{I}_{K_5}, & n = 1, 2, 3, 4; \\ \mathbf{I}_{N_1} \otimes \dots \otimes \mathbf{I}_{N_4} \otimes \check{\mathbf{J}}_{5,i}, & n = 5; \end{cases}$$

with the modified selection matrices  $\mathbf{L}_{n,1}$  and  $\mathbf{L}_{n,2}$  given in (12) and (13), respectively, and

$$\check{\mathbf{J}}_{5,i} = \begin{cases} [\mathbf{I}_{K_5-1}, \mathbf{0}_{(K_5-1) \times 1}], & i = 1; \\ [\mathbf{0}_{(K_5-1) \times 1}, \mathbf{I}_{K_5-1}], & i = 2. \end{cases}$$

*Proof.* The proof can be found in Appendix B-A.  $\square$

Proposition 2 indicates that the shift invariance properties can be perfectly restored if the transformation matrix in each mode has the desired shift invariance structure. When the shift invariance structure does not hold, i.e.,  $\mathbf{J}_{n,1} \mathbf{T}_n \neq \mathbf{J}_{n,2} \mathbf{T}_n \mathbf{F}_n$ , we can find an approximate non-singular matrix  $\tilde{\mathbf{F}}_n$ , such that  $\mathbf{J}_{n,1} \mathbf{T}_n \approx \mathbf{J}_{n,2} \mathbf{T}_n \tilde{\mathbf{F}}_n$  as before. After that, the approximation  $\tilde{\mathbf{F}}_n$  is used in proposition 2. Therefore, the proposed framework can be applied to system with arbitrary beamforming and combination matrices.

Performing singular value decomposition on  $\mathbf{H}$ , we have

$$\mathbf{H} = \mathbf{U}_s \Sigma_s \mathbf{V}_s^H, \quad (20)$$

where the  $L$  leading left singular vectors in  $\mathbf{U}_s$  span the column space of  $\mathbf{H}$ . Note the same space is spanned by the columns of  $\mathbf{P}$ , we then have a non-singular matrix  $\mathbf{E} \in \mathbb{C}^{L \times L}$  such that  $\mathbf{P} = \mathbf{U}_s \mathbf{E}$ . Substituting into (19), we have

$$\check{\mathbf{J}}_{n,1} \mathbf{U}_s \tilde{\Gamma}_n = \check{\mathbf{J}}_{n,2} \mathbf{U}_s, \quad (21)$$

where  $\tilde{\Gamma}_n \in \mathbb{C}^{L \times L}$  is given by

$$\tilde{\Gamma}_n = \mathbf{E} \check{\Phi}_n \mathbf{E}^{-1}. \quad (22)$$

The least-square solution of  $\tilde{\Gamma}_n$  from (21) can be obtained as

$$\tilde{\Gamma}_n \approx (\check{\mathbf{J}}_{n,1} \mathbf{U}_s)^\dagger \check{\mathbf{J}}_{n,2} \mathbf{U}_s. \quad (23)$$

We perform the eigenvalue decomposition on  $\tilde{\Gamma}_n$  obtained from (23), and the angular frequency in each dimension can be obtained through the eigenvalues as indicated by (22).

### C. Channel Parameter Estimation

The independent eigenvalue decomposition operations in each mode cannot achieve auto-pairing. Moreover, when identical or very close angular frequencies in the  $n$ -th mode is present, the eigenvectors corresponding to the same eigenvalues cannot be distinguished. This could happen, for example, with close scatterer points in the environments. To achieve auto-pairing of the angular frequencies crossing all dimensions, we construct a new matrix  $\mathbf{K} \in \mathbb{C}^{L \times L}$  as

$$\mathbf{K} = \sum_{n=1}^N \beta_n \tilde{\Gamma}_n, \quad (24)$$

### Algorithm 2 Matrix-based Beamspace ESPRIT Approach for Channel Parameter Estimation

**Input:** Noisy beamspace observation in vector  $\tilde{\mathbf{h}}^{(b)} = \text{vec}_r \left\{ \hat{\mathcal{H}}^{(b)} \right\};$

**Output:** Channel parameter estimates:  $\phi_{\text{el}}^l, \phi_{\text{az}}^l, \theta_{\text{el}}^l, \theta_{\text{az}}^l, \tau_l$ , and  $\gamma_l$ , for  $l = 1, 2, \dots, L$ .

- 1: Choose  $L_5$  and let  $K_5 \leftarrow M_5 + 1 - L_5$ ;
- 2: Construct the matrix  $\tilde{\mathbf{H}}$  according to (15) with  $\tilde{\mathbf{h}}^{(b)}$ ;
- 3: Perform the SVD of  $\tilde{\mathbf{H}}$ , and extract the signal subspace  $\tilde{\mathbf{U}}_s$  with the leading  $L$  singular vectors;
- 4: Compute  $\tilde{\Gamma}_n$  from (23) for  $n = 1, 2, \dots, N$  with  $\tilde{\mathbf{U}}_s$ ;
- 5: Generate random  $\beta$ , and compute  $\tilde{\mathbf{K}}$  from (24);
- 6: Perform the ED of  $\tilde{\mathbf{K}}$  to extract  $\tilde{\mathbf{E}}$  as shown in (25);
- 7: Apply  $\tilde{\mathbf{E}}$  to compute  $\tilde{\Psi}_n$  from (26) for  $n = 1, 2, \dots, N$ ;
- 8: Estimate the angular frequencies  $\hat{\omega}_{l,n}$  from (27);
- 9: Obtain the channel parameter estimates.

where  $\beta = [\beta_1, \beta_2, \dots, \beta_N]^T$  is a random vector. With the results in (22), we have

$$\mathbf{K} = \sum_{n=1}^N \beta_n \mathbf{E} \check{\Phi}_n \mathbf{E}^{-1} = \mathbf{E} \mathbf{\Lambda} \mathbf{E}^{-1}, \quad (25)$$

where  $\mathbf{\Lambda} \in \mathbb{C}^{L \times L}$  is a diagonal matrix given by  $\mathbf{\Lambda} = \sum_{n=1}^N \beta_n \check{\Phi}_n$ . This indicates that even if the angular frequencies in the  $n$ -th dimension are the same, the diagonal elements in  $\mathbf{\Lambda}$  can be likely distinct, since the angular frequencies in other dimensions can be different. As a result, instead of applying eigenvalue decomposition operations on each  $\tilde{\Gamma}_n$ , we only need to perform one eigenvalue decomposition on  $\mathbf{K}$ . As long as the diagonal elements in  $\mathbf{\Lambda}$  are distinct from each other, a unique  $\mathbf{E}$  can be obtained, which is used to recover the angular frequencies in each mode. This leads to auto-pairing of angular frequencies in all dimensions. With the acquisition of  $\mathbf{E}$ , from (22), we have

$$\tilde{\Phi}_n = \mathbf{E}^{-1} \tilde{\Gamma}_n \mathbf{E}. \quad (26)$$

The angular frequency  $\omega_{l,n}$  is obtained as

$$\omega_{l,n} = \Im \{ \ln(\tilde{\Phi}_{l,n}) \}. \quad (27)$$

With the estimated angular frequencies, we reconstruct the matrix  $\hat{\mathbf{B}} \in \mathbb{C}^{N_1 N_2 \dots N_5 \times L}$  as

$$\hat{\mathbf{B}} = \hat{\mathbf{B}}_1^{(N_1)} \circ \hat{\mathbf{B}}_2^{(N_2)} \circ \dots \circ \hat{\mathbf{B}}_4^{(N_4)} \circ \hat{\mathbf{A}}_5^{(M_5)}, \quad (28)$$

where  $\hat{\mathbf{B}}_n^{(N_n)}$  is computed from (4). The corresponding channel parameters associated with each propagation path can be obtained from the one-to-one mapping and  $\hat{\gamma} = (\hat{\mathbf{B}})^\dagger \tilde{\mathbf{h}}^{(b)}$ . The matrix-based beamspace ESPRIT algorithm is presented in Algorithm 2.

### D. Variations of the Hybrid ESPRIT Approaches

When  $\mathbf{T}_n$  does not hold the shift-invariance properties, the approximation  $\tilde{\mathbf{F}}_n$  from the least-square solution requires the full-column rank conditions of  $\mathbf{J}_{n,2} \mathbf{T}_n$ . However, if the conditions are not valid, for example, in the case  $M_n < N_n$ , we

can apply the hybrid ESPRIT approaches instead. Specifically, when  $M_n < N_n$ , and  $\mathbf{T}_n$  is full-row rank<sup>2</sup>, we define the tensor  $\check{\mathcal{H}}_n \in \mathbb{C}^{N_1 \times \dots \times M_n \times \dots \times N_5}$  as the  $n$ -th mode product of  $\mathcal{H}^{(b)}$  and the matrix  $(\mathbf{T}_n^H)^\dagger$ , i.e.,

$$\check{\mathcal{H}}_n = \mathcal{H}^{(b)} \times_n (\mathbf{T}_n^H)^\dagger. \quad (29)$$

As a result, the corresponding canonical polyadic model of  $\check{\mathcal{H}}_n$  can be given as

$$\check{\mathcal{H}}_n = \sum_{l=1}^L \gamma_l \mathbf{b}^{(N_1)}(\omega_{l,1}) \circ \dots \circ \mathbf{a}^{(M_n)}(\omega_{l,n}) \circ \dots \circ \mathbf{b}^{(N_5)}(\omega_{l,5}),$$

where we have applied the results  $(\mathbf{T}_n^H)^\dagger \mathbf{T}_n^H = \mathbf{I}_{M_n}$ . Therefore, the angular frequency estimation in the  $n$ -th mode can be obtained through the element-space ESPRIT approaches as we have done in the frequency domain. For simplicity, we use the new selection matrices  $\mathbf{L}_{n,1} \in \mathbb{C}^{(M_n-1) \times M_n}$  and  $\mathbf{L}_{n,2} \in \mathbb{C}^{(M_n-1) \times M_n}$  as

$$\mathbf{L}_{n,i} = \begin{cases} \begin{bmatrix} \mathbf{I}_{M_n-1}, \mathbf{0}_{(M_n-1) \times 1} \end{bmatrix}, & i = 1; \\ \begin{bmatrix} \mathbf{0}_{(M_n-1) \times 1}, \mathbf{I}_{M_n-1} \end{bmatrix}, & i = 2, \end{cases}$$

and  $\check{\mathcal{H}}_n$  in the matrix-based beamspace ESPRIT approaches. This process can be repeated if the shift invariance properties does not hold in multiple  $\mathbf{T}_n$ , hence we refer the new approach as to the hybrid ESPRIT approach.

### E. Reduced-Complexity Matrix-Based Beamspace ESPRIT

By exploiting the structure of  $\tilde{\mathbf{H}}$ , we propose a low-complexity SVD algorithm, which is the computational bottleneck in Algorithm 2.

1) *Proposed SVD algorithm:* To begin with, we define a set of matrices  $\tilde{\mathbf{H}}_{n_1, n_2, n_3, n_4} \in \mathbb{C}^{K_5 \times L_5}$  as

$$\tilde{\mathbf{H}}_{n_1, n_2, n_3, n_4} = \begin{bmatrix} \tilde{h}_{n_1, n_2, n_3, n_4, 1}^{(b)} & \dots & \tilde{h}_{n_1, n_2, n_3, n_4, L_5}^{(b)} \\ \vdots & \ddots & \vdots \\ \tilde{h}_{n_1, n_2, n_3, n_4, K_5}^{(b)} & \dots & \tilde{h}_{n_1, n_2, n_3, n_4, N_5}^{(b)} \end{bmatrix}.$$

It immediately arrives that the matrix  $\tilde{\mathbf{H}}$  can be constructed as

$$\tilde{\mathbf{H}} = \begin{bmatrix} \tilde{\mathbf{H}}_{1,1,1,1} \\ \tilde{\mathbf{H}}_{1,1,1,2} \\ \vdots \\ \tilde{\mathbf{H}}_{1,1,2,1} \\ \vdots \\ \tilde{\mathbf{H}}_{N_1, N_2, N_3, N_4} \end{bmatrix}.$$

The SVD of  $\tilde{\mathbf{H}}$  consists of two steps: Lanczos bidiagonalization and the SVD of bidiagonalization matrix. Specifically, the Lanczos bidiagonalization is to transform  $\tilde{\mathbf{H}}$  into an upper bidiagonal matrix  $\mathbf{J} \in \mathbb{C}^{L_5 \times L_5}$  as  $\mathbf{J} = \mathbf{U}_L^H \tilde{\mathbf{H}} \mathbf{V}_L$ , where  $\mathbf{U}_L \in \mathbb{C}^{N_1 N_2 N_3 N_4 K_5 \times L_5}$ , and  $\mathbf{V}_L \in \mathbb{C}^{L_5 \times L_5}$  satisfying  $\mathbf{U}_L^H \mathbf{U}_L = \mathbf{V}_L \mathbf{V}_L^H = \mathbf{V}_L^H \mathbf{V}_L = \mathbf{I}_{L_5}$ . Let  $\mathbf{U}_L = [\mathbf{u}_1, \mathbf{u}_2, \dots, \mathbf{u}_{L_5}]$ , and  $\mathbf{V}_L = [\mathbf{v}_1, \mathbf{v}_2, \dots, \mathbf{v}_{L_5}]$ . The upper bidiagonal matrix  $\mathbf{J}$  can

be represented by two vectors, i.e.,  $\mathbf{a} = [a_1, a_2, \dots, a_{L_5}]^T$  and  $\mathbf{b} = [b_1, b_2, \dots, b_{L_5-1}]^T$ , and

$$\mathbf{J} = \begin{bmatrix} a_1 & b_1 & & \dots & 0 \\ & & \ddots & \ddots & \\ & & & \ddots & b_{L_5-1} \\ 0 & \dots & & & a_{L_5} \end{bmatrix}.$$

The vectors  $\mathbf{u}_{\ell_5}$  and  $\mathbf{v}_{\ell_5}$  can be obtained through the Lanczos recursions, i.e.,

$$a_{\ell_5} \mathbf{u}_{\ell_5} = \tilde{\mathbf{H}} \mathbf{v}_{\ell_5} - b_{\ell_5-1} \mathbf{u}_{\ell_5-1}, \quad (30)$$

$$b_{\ell_5} \mathbf{v}_{\ell_5+1} = \tilde{\mathbf{H}}^H \mathbf{u}_{\ell_5} - a_{\ell_5} \mathbf{v}_{\ell_5}, \quad (31)$$

given the initialization vector  $\mathbf{u}_0$  and  $b_0$ . After the Lanczos bidiagonalization, we perform the SVD of  $\mathbf{J}$ , i.e.,

$$\mathbf{J} = \mathbf{U}_J \Sigma_J \mathbf{V}_J^H, \quad (32)$$

where both  $\mathbf{U}_J \in \mathbb{C}^{L_5 \times L_5}$  and  $\mathbf{V}_J \in \mathbb{C}^{L_5 \times L_5}$  are unitary matrices. As a result, the left unitary matrix corresponding to the SVD of  $\tilde{\mathbf{H}}$  can be obtained as

$$\mathbf{U}_H = \mathbf{U}_L \mathbf{U}_J, \quad (33)$$

and the leading  $L$  singular vectors in  $\mathbf{U}_H$  are extracted as signal subspace, i.e.,  $\tilde{\mathbf{U}}_s = (\mathbf{U}_H)_{:,1:L}$ . Note  $\tilde{\mathbf{H}}_{n_1, n_2, n_3, n_4}$  is a Hankel matrix, and the matrix-vector product can be efficiently implemented with fast Fourier transform (FFT) and inverse-FFT (IFFT) algorithms [26], [27]. As a result, the SVD of  $\tilde{\mathbf{H}}$  can be implemented efficiently.

2) *Complexity Analysis:* In Algorithm 2, we notice that the main complexity comes from the SVD of  $\tilde{\mathbf{H}}$ . From [26], [27], the matrix-vector product for  $\tilde{\mathbf{H}}_{n_1, n_2, n_3, n_4}$  can be efficiently implemented with  $\mathcal{O}(N_5 \log N_5)$  computations. Therefore, the matrix-vector product for  $\tilde{\mathbf{H}}$  requires  $\mathcal{O}(J \log N_5)$  computations where  $J = N_1 N_2 N_3 N_4 N_5$ . The Lanczos bidiagonalization process can be implemented with  $\mathcal{O}(J N_5 \log N_5)$ . In addition, the SVD of a bidiagonal matrix can be implemented with  $\mathcal{O}(N_5^2)$ . Therefore, the overall complexity to perform the SVD of  $\tilde{\mathbf{H}}$  is  $\mathcal{O}(J N_5 \log N_5)$ . However, we only need to extract the  $L$  leading singular vectors; therefore, the overall complexity is further reduced to  $\mathcal{O}(L J \log N_5)$ , which is almost linearly with the  $LJ$ . On the other hand, the major computations in Algorithm 1 comes from the CP decomposition of the tensor  $\hat{\mathcal{H}}^{(b)}$  with the size of  $N_1 \times N_2 \times N_3 \times N_4 \times M_5$ , which requires  $\mathcal{O}(2^N L J + N L^3)$  if the alternating least squares (ALS) algorithm with line search is used [22]. As indicated in [17], the tensor-based approaches have the complexity in the same order of the matrix based approaches, but require much more computations, which will be demonstrated in Section VI-D by evaluating the program running time.

## V. PERTURBATION ANALYSIS

In this section, we provide the closed-form analytical performance of the channel parameter and location estimation. This can be done by performing the first-order perturbation analysis. It is worth pointing out that the proposed method does not require the statistical knowledge of the noise component since it is directly applied to the beamspace observations. As a

<sup>2</sup>In the design of the transform matrix  $\mathbf{T}_n$ , we can easily meet the full rank conditions. When using random beams in the system, the full rank conditions are satisfied with high probability.

result, the Cramér–Rao bound (CRB) may not be available if noise statistics are unknown. In addition, as the noise component is not considered, the performance gap between the ESPRIT approaches and the CRB has been clearly identified in existing literature [11], [17], [28], [29]. On the other hand, the first-order perturbation analysis, as we will show in the next section, matches well with the simulations, which is more meaningful to demonstrate the estimation performance of the proposed method.

#### A. First-order Perturbation of Channel Parameter Estimation

With  $\mathbf{h}^{(b)}$ , we construct the noiseless matrix  $\mathbf{H}$  from (15). The SVD of  $\mathbf{H}$  is given by

$$\mathbf{H} = \mathbf{U}_s \mathbf{\Sigma}_s \mathbf{V}_s^H + \mathbf{U}_n \mathbf{\Sigma}_n \mathbf{V}_n^H, \quad (34)$$

and  $\mathbf{\Sigma}_n = \mathbf{0}$ . The estimates,  $\tilde{\mathbf{H}}$  is expressed as

$$\tilde{\mathbf{H}} = \mathbf{H} + \Delta\mathbf{H}, \quad (35)$$

where  $\Delta\mathbf{H} = \mathcal{S}(\Delta\mathbf{h})$ , and  $\Delta\mathbf{h} \in \mathbb{C}^{N_1 N_2 N_3 N_4 M_5}$  is the beamspace channel estimation error.

With the noisy estimates, the first-order perturbation  $\Delta\Phi_{l,n} = \tilde{\Phi}_{l,n} - \Phi_{l,n}$  from the proposed algorithm is given as follows.

**Lemma 1.**  $\Delta\Phi_{l,n}$  is given by

$$\Delta\Phi_{l,n} = \frac{1}{\gamma_l} \mathbf{b}_l^T (\check{\mathbf{J}}_{n,1} \mathbf{P})^\dagger (\check{\mathbf{J}}_{n,2} - \Phi_{l,n} \check{\mathbf{J}}_{n,1}) \Delta\mathbf{H} (\mathbf{G}^T)^\dagger \mathbf{b}_l, \quad (36)$$

where  $\mathbf{b}_l$  is the  $l$ -th column of  $\mathbf{I}_L$ . The matrix  $\mathbf{P}$  and  $\mathbf{G}$  are given by (17) and (18), respectively.

*Proof.* The proof can be found in Appendix C-A.  $\square$

Denote  $\boldsymbol{\chi}_l \in \mathbb{C}^{L_5 \times 1}$  and  $\boldsymbol{\lambda}_{l,n} \in \mathbb{C}^{N_1 N_2 N_3 N_4 K_5 \times 1}$  as

$$\boldsymbol{\lambda}_{l,n}^H = \mathbf{b}_l^T (\check{\mathbf{J}}_{n,1} \mathbf{P})^\dagger (\check{\mathbf{J}}_{n,2} - \Phi_{l,n} \check{\mathbf{J}}_{n,1}), \quad (37)$$

$$\boldsymbol{\chi}_l^* = (\mathbf{G}^T)^\dagger \mathbf{b}_l. \quad (38)$$

The vector  $\boldsymbol{\lambda}_{l,n}$  can also be represented by

$$\boldsymbol{\lambda}_{l,n} = \left[ \left( \boldsymbol{\lambda}_{l,n}^{(1,1,1,1)} \right)^T, \left( \boldsymbol{\lambda}_{l,n}^{(1,1,1,2)} \right)^T, \dots, \left( \boldsymbol{\lambda}_{l,n}^{(1,1,1,N_1)} \right)^T, \right. \\ \left. \left( \boldsymbol{\lambda}_{l,n}^{(1,1,2,1)} \right)^T, \dots, \left( \boldsymbol{\lambda}_{l,n}^{(N_1, N_2, N_3, N_4)} \right)^T \right]^T, \quad (39)$$

where  $\boldsymbol{\lambda}_{l,n}^{(n_1, n_2, n_3, n_4)} \in \mathbb{C}^{K_5 \times 1}$ . We further define  $\boldsymbol{\xi}_{l,n}$  as

$$\boldsymbol{\xi}_{l,n} = \left[ \left( \boldsymbol{\xi}_{l,n}^{(1,1,1,1)} \right)^T, \left( \boldsymbol{\xi}_{l,n}^{(1,1,1,2)} \right)^T, \dots, \left( \boldsymbol{\xi}_{l,n}^{(1,1,1,N_1)} \right)^T, \right. \\ \left. \left( \boldsymbol{\xi}_{l,n}^{(1,1,2,1)} \right)^T, \dots, \left( \boldsymbol{\xi}_{l,n}^{(N_1, N_2, N_3, N_4)} \right)^T \right]^T, \quad (40)$$

where  $\boldsymbol{\xi}_{l,n}^{(n_1, n_2, n_3, n_4)} \in \mathbb{C}^{M_5 \times 1}$  is the convolution of  $\boldsymbol{\lambda}_{l,n}^{(n_1, n_2, n_3, n_4)}$  and  $\boldsymbol{\chi}_l$ . We then have the following proposition.

**Proposition 3.** With the beamspace channel estimation error  $\Delta\mathbf{h}$ , the first-order perturbation  $\Delta\Phi_{l,n}$  in (36) is equivalent to

$$\Delta\Phi_{l,n} = \frac{\boldsymbol{\xi}_{l,n}^H \Delta\mathbf{h}}{\gamma_l}, \quad (41)$$

where  $\boldsymbol{\xi}_{l,n}$  is given by (40).

*Proof.* The proof can be found in Appendix C-B.  $\square$

*Remarks:* Compared to the first-order perturbation expression in Lemma 1, the results in Proposition 3 has a two-fold merit. First of all, the expression in (41) simplifies the first-order perturbation  $\Delta\Phi_{l,n}$  in (36), enabling the perturbation analysis without knowing  $\Delta\mathbf{H}$ . Secondly, equation (41) also simplifies the analysis of the statistic properties (including the mean and variance) of the estimation errors. The latter one is more important in the perturbation analysis of the complex gain and position estimation.

From (27), the perturbation of  $\omega_{l,n}$  is readily given by

$$\Delta\omega_{l,n} = \Im \{ \mathbf{v}_{l,n}^H \Delta\mathbf{h} \}, \quad (42)$$

where  $\mathbf{v}_{l,n} = \Phi_{l,n} \boldsymbol{\xi}_{l,n} / \gamma_l^*$ .

We are now able to give the first-order perturbation of the channel parameters for each path.

**Lemma 2.** The first-order perturbations of the channel parameters can be given as

$$\Delta\phi_{az}^l = \Im \{ \boldsymbol{\kappa}_{l,1}^H \Delta\mathbf{h} \}, \Delta\phi_{el}^l = \Im \{ \boldsymbol{\kappa}_{l,2}^H \Delta\mathbf{h} \}, \quad (43)$$

$$\Delta\theta_{az}^l = \Im \{ \boldsymbol{\kappa}_{l,3}^H \Delta\mathbf{h} \}, \Delta\theta_{el}^l = \Im \{ \boldsymbol{\kappa}_{l,4}^H \Delta\mathbf{h} \}, \quad (44)$$

$$\Delta\tau_l = \Im \{ \boldsymbol{\kappa}_{l,5}^H \Delta\mathbf{h} \}, \quad (45)$$

$$\Delta\gamma_l = \mathbf{b}_l^T \mathbf{B}^\dagger \Delta\mathbf{h} - \sum_{n=1}^5 \mathbf{b}_l^T \boldsymbol{\Upsilon}_n \Im \{ \mathbf{V}_n^H \Delta\mathbf{h} \}, \quad (46)$$

where  $\mathbf{V}_n = [\mathbf{v}_{1,n}, \mathbf{v}_{2,n}, \dots, \mathbf{v}_{L,n}]$ . The matrix  $\boldsymbol{\kappa}_{l,i} \in \mathbb{C}^{N_1 N_2 N_3 N_4 M_5 \times 1}$ , and  $\boldsymbol{\Upsilon}_n \in \mathbb{C}^{N_1 N_2 N_3 N_4 M_5 \times L}$  are given as

$$\boldsymbol{\kappa}_{l,1} = \frac{\mathbf{v}_{l,1}}{\pi \cos(\phi_{az}^l) \sin(\phi_{el}^l)} + \frac{\sin(\phi_{az}^l) \cos(\phi_{el}^l) \mathbf{v}_{l,2}}{\pi \cos(\phi_{az}^l) \sin^2(\phi_{el}^l)}, \quad (47)$$

$$\boldsymbol{\kappa}_{l,2} = \frac{\mathbf{v}_{l,2}}{\pi \sin(\phi_{el}^l)}, \quad (48)$$

$$\boldsymbol{\kappa}_{l,3} = \frac{\mathbf{v}_{l,3}}{\pi \cos(\theta_{az}^l) \sin(\theta_{el}^l)} + \frac{\sin(\theta_{az}^l) \cos(\theta_{el}^l) \mathbf{v}_{l,4}}{\pi \cos(\theta_{az}^l) \sin^2(\theta_{el}^l)}, \quad (49)$$

$$\boldsymbol{\kappa}_{l,4} = \frac{\mathbf{v}_{l,4}}{\pi \sin(\theta_{el}^l)}, \boldsymbol{\kappa}_{l,5} = \frac{\mathbf{v}_{l,5}}{2\pi \Delta f}, \quad (50)$$

$$\boldsymbol{\Upsilon}_n = \mathbf{B}^\dagger \check{\mathbf{B}}_n \odot \boldsymbol{\gamma}^T, \quad (51)$$

where  $\mathbf{B}$  is given by (28) and  $\check{\mathbf{B}}_n$  is given by (70).

*Proof.* The proof can be found in Appendix C-C.  $\square$

In addition, when the beamspace channel estimation error is complex circular Gaussian, we have the following proposition.

**Proposition 4.** With the proposed algorithm, the expectation and covariance of the first-order perturbation of the channel

parameter estimation are given as

$$\mathbb{E}(\Delta\phi_{az}^l) = 0, \quad \mathbb{E}(\|\Delta\phi_{az}^l\|^2) = \frac{N_0 \|\boldsymbol{\kappa}_{l,1}\|^2}{2N_p E_s} \quad (52)$$

$$\mathbb{E}(\Delta\phi_{el}^l) = 0, \quad \mathbb{E}(\|\Delta\phi_{el}^l\|^2) = \frac{N_0 \|\boldsymbol{\kappa}_{l,2}\|^2}{2N_p E_s}, \quad (53)$$

$$\mathbb{E}(\Delta\theta_{az}^l) = 0, \quad \mathbb{E}(\|\Delta\theta_{az}^l\|^2) = \frac{N_0 \|\boldsymbol{\kappa}_{l,3}\|^2}{2N_p E_s}, \quad (54)$$

$$\mathbb{E}(\Delta\theta_{el}^l) = 0, \quad \mathbb{E}(\|\Delta\theta_{el}^l\|^2) = \frac{N_0 \|\boldsymbol{\kappa}_{l,4}\|^2}{2N_p E_s}, \quad (55)$$

$$\mathbb{E}(\Delta\tau_l) = 0, \quad \mathbb{E}(\|\Delta\tau_l\|^2) = \frac{N_0 \|\boldsymbol{\kappa}_{l,5}\|^2}{2N_p E_s}, \quad (56)$$

$$\mathbb{E}(\Delta\gamma_l) = 0, \quad \mathbb{E}(\|\Delta\gamma_l\|^2) = \frac{N_0 \|\boldsymbol{\Pi}_l\|_F^2}{2N_p E_s}, \quad (57)$$

where  $\boldsymbol{\kappa}_{l,i}$ ,  $i = 1, 2, 3, 4, 5$ , is given in Lemma 2, and  $\|\cdot\|_F$  is the Frobenius norm.  $\boldsymbol{\Pi}_l$  is given by

$$\boldsymbol{\Pi}_l = \begin{bmatrix} \Re\{\mathbf{b}_l^T \mathbf{B}^\dagger\} & -\Im\{\mathbf{b}_l^T \mathbf{B}^\dagger\} \\ \Im\{\mathbf{b}_l^T \mathbf{B}^\dagger\} & \Re\{\mathbf{b}_l^T \mathbf{B}^\dagger\} \end{bmatrix} - \sum_{n=1}^5 \begin{bmatrix} \Re\{\mathbf{b}_l^T \boldsymbol{\Upsilon}_n\} \\ \Im\{\mathbf{b}_l^T \boldsymbol{\Upsilon}_n\} \end{bmatrix} \begin{bmatrix} \Im\{\mathbf{V}_n^H\} & \Re\{\mathbf{V}_n^H\} \end{bmatrix}. \quad (58)$$

*Proof.* The results are straightforward based on Lemma 2.  $\square$

### B. First-order Perturbation of Position Estimation

With the estimates of the channel parameters, we perform the positioning with the method in Section II-C1. Given the first-order perturbation of the channel parameters, we obtain the first-order perturbation of the position estimation as follows.

**Lemma 3.** *The first-order perturbation of the position estimate,  $\Delta\mathbf{p}_R = \hat{\mathbf{p}}_R - \mathbf{p}_R$ , is given by*

$$\Delta\mathbf{p}_R = \Im\{\boldsymbol{\Psi} \Delta\mathbf{h}\}, \quad (59)$$

where  $\boldsymbol{\Psi} \in \mathbb{C}^{3 \times N_1 N_2 N_3 N_4 M_5}$  is given by

$$\boldsymbol{\Psi} = \sum_{l=1}^L \check{\mathbf{D}}_l [\boldsymbol{\kappa}_{l,3}, \boldsymbol{\kappa}_{l,4}, \boldsymbol{\kappa}_{l,5}]^H + \check{\mathbf{E}}_l [\boldsymbol{\kappa}_{l,1}, \boldsymbol{\kappa}_{l,2}, \boldsymbol{\kappa}_{l,3}, \boldsymbol{\kappa}_{l,4}, \boldsymbol{\kappa}_{l,5}]^H, \quad (60)$$

where  $\boldsymbol{\kappa}_{l,i}$ ,  $i = 1, 2, 3, 4, 5$ , are given in Lemma 2.  $\check{\mathbf{D}}_l \in \mathbb{R}^{3 \times 3}$  and  $\check{\mathbf{E}}_l \in \mathbb{R}^{3 \times 5}$  are given by (82) and (83), respectively.

*Proof.* The proof can be found in Appendix C-D.  $\square$

When the beamspace channel estimation error is complex circular Gaussian, we have the following proposition.

**Proposition 5.** *With the proposed positioning method, the expectation and covariance of the first-order perturbation of the position estimate are given by*

$$\mathbb{E}(\Delta\mathbf{p}_R) = \mathbf{0}, \quad \mathbb{E}(\|\Delta\mathbf{p}_R\|^2) = \frac{N_0 \|\boldsymbol{\Psi}\|_F^2}{2N_p E_s}. \quad (61)$$

*Proof.* The results are straightforward based on Lemma 3.  $\square$

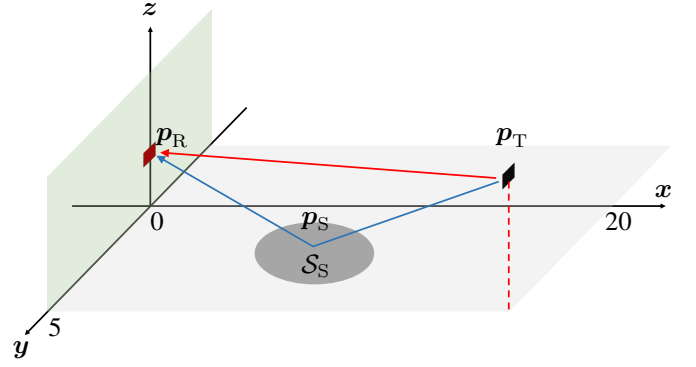


Fig. 2: Simulation setup: 1 LOS and 1 NLOS paths, scatter point  $\mathbf{p}_S$  located at the the gray region  $\mathcal{S}_S$ . The base station and vehicular user are equipped with URAs in  $y-z$  plane.

TABLE I: Parameters in Simulations

Parameters	Values
Carrier frequency $f_c$	30 GHz
Bandwidth	400 MHz
Subcarrier spacing $\Delta f$	120 kHz
Number of subcarriers $M_5$	500
Wavelength $\lambda$	1 cm
Size of URA at transmitter $M_1 \times M_2$	$8 \times 8$
Size of URA at receiver $M_3 \times M_4$	$8 \times 8$
Antenna spacing $\Delta d$	0.5 cm
Number of RF chains at transmitter $N_T$	16
Number of RF chains at receiver $N_R$	16
Number of transmit beams $N_1 \times N_2$	$4 \times 4$
Number of receive beams $N_3 \times N_4$	$4 \times 4$
Base station location $\mathbf{p}_T$	$[20, 5, 8]^T$
Number of pilots $N_P$	32
Coherence time	5 ms

## VI. PERFORMANCE EVALUATION AND DISCUSSIONS

### A. Simulation Setup

In the simulations, we consider the simultaneous localization and communications for a vehicular user, with simulation parameters in Table I. Specifically, we consider one line-of-sight (LOS) and NLOS path from the ground as shown in Fig. 2. We denote  $\mathcal{S}_S \triangleq \{(x, y, z) \in \mathbb{R}^3 | z = 0, (x - 10)^2 + (y - 2.5)^2 \leq r_S^2\}$  as the area where the scatter point is located. The coherence time is set to 5 ms, indicating 600 coherent OFDM blocks. Among them, the first  $N_P$  OFDM blocks are used for pilot transmission, while the remaining blocks are used for data transmission. The overall bandwidth of the system is 400 MHz, using 3300 subcarriers starting from 28 GHz. Among them, we use the every 6-th subcarrier for pilot transmission. As examples to validate the performance of the proposed method, we evaluate the estimation performance with both the DFT beams (with beam separation of  $\pi/4$  in each dimension) and the directional beams with a closer beam separation of  $\pi/8$  at both transmitter and receiver sides. The estimation of the clock bias and orientation of the vehicular user is out of the scope in this work that we assume perfect synchronization and known orientation at receiver in the framework. All simulations are performed in MATLAB on a laptop with a 2.3 GHz Quad-Core Intel Core i7 processor and 16 GB memory.



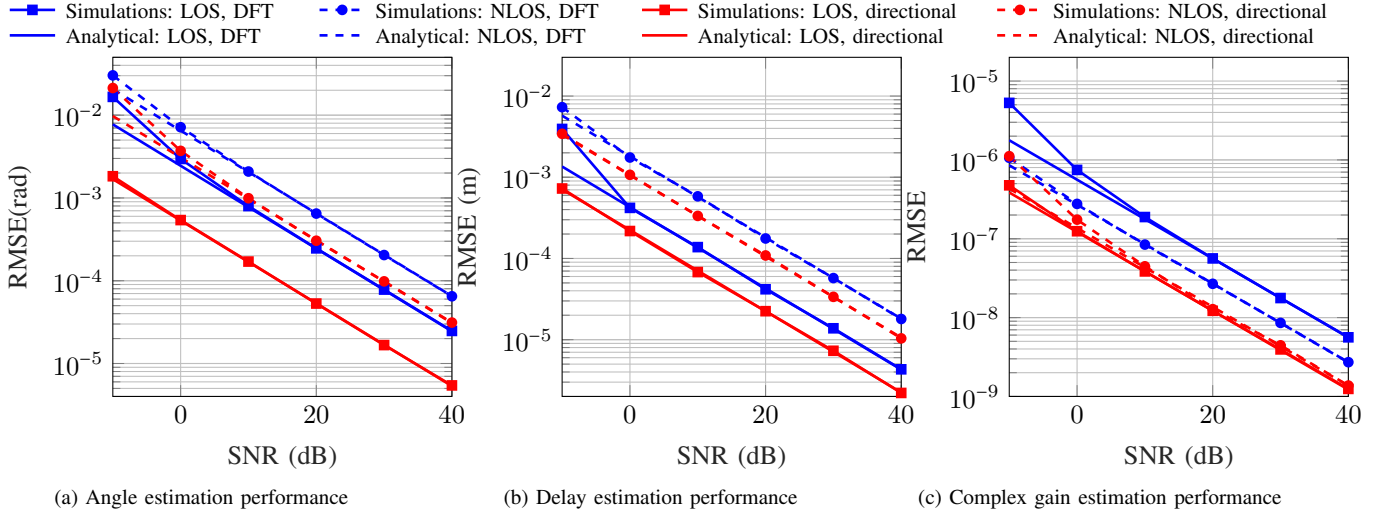


Fig. 3: Analytical performance validation: 1 LOS path and 1 NLOS path,  $N_P = 32$ , DFT beams and directional beams.

The geometric relationship between the positions and the angles/delays are the same as that in [6], [22]. The path loss  $\rho_l$  for the  $l$ -th path follows the models in [6], [22], given by

$$\rho_l \propto \varsigma_l \left( \frac{\lambda}{4\pi d_l} \right)^2, \quad (62)$$

where  $d_l$  is the propagation distance, and  $\varsigma_l$  indicates the power of the  $l$ -th multipath component after scattering. The SNR at receiver side before signal combination is given by

$$\text{SNR} = \frac{\sum_{m_5=1}^{M_5} \|\mathbf{H}_{m_5} \mathbf{F}\|_F^2 E_s}{\sum_{m_5=1}^{M_5} \mathbb{E}(\|\mathbf{Z}_{m_5}\|^2)}, \quad (63)$$

where  $\mathbf{H}_{m_5} \in \mathbb{C}^{M_3 M_4 \times M_1 M_2}$  is the channel matrix over the  $m_5$ -th subcarrier.

For evaluation, we use the root mean-square error metric for both channel parameter and position estimation and compare to the closed-form first-order perturbation analytical results. In addition, we also compare the estimation and complexity performance of the proposed scheme to the existing tensor decomposition method in [20], [21].

### B. Channel Parameter Estimation Performance

We first evaluate the analytical perturbation performance and the numerical performance of the proposed beamspace ESPRIT approach with the system configuration given in Table I. In Fig. 3, we present the channel parameter estimation performance with both the DFT beams and the directional beams in each mode at transmitter and receiver sides.<sup>3</sup> The following observations can be seen from Fig. 3.

- The analytical and numerical results for channel parameter estimation show to be well-matched, particularly in high SNR regions. This is consistent with the first-order perturbation analysis, since higher-order perturbations can be reasonably ignored when SNR is high.

<sup>3</sup>The transformation matrices are selected to cover the area of interest in the setup. In this case, the selections are made with the prior user and scatter location information.

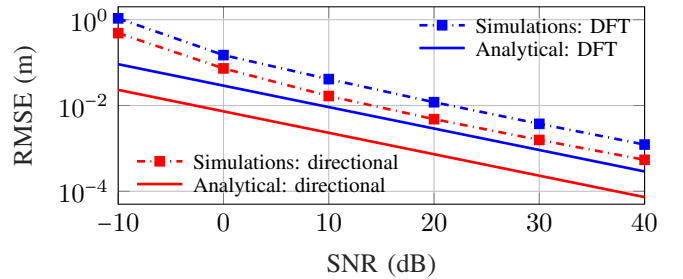


Fig. 4: Localization performance: DFT beams and directional beams, 1 LOS and 1 NLOS,  $N_P = 32$ .

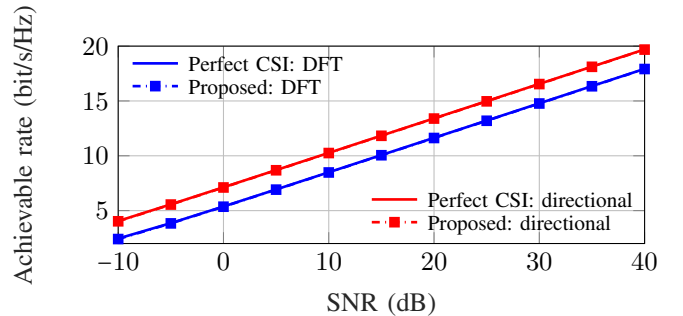


Fig. 5: Achievable rate performance: 1 LOS and 1 NLOS,  $N_P = 32$ , DFT beams and directional beams.

- The angle and delay estimations of the LOS path are better than that of the NLOS components. This is reasonable as the LOS path has relatively higher SNR.
- The channel parameter estimation performance is significantly improved if the directional beams with closer beam separation is used. Particularly, if the directional beams with closer separation are used, the effective SNR can be boosted and the angle estimation performance is significantly improved, leading to the improvement of other channel parameter estimation performance.

The first-order perturbation of angular frequency estimation has been widely studied in the literature, for example, [11], [13], [17], [28]–[30]; however, it is worth pointing out that the first-order perturbation of the channel parameter estimation, especially the complex gain estimation, is rarely studied. Our closed-form first-order perturbation of the channel parameter estimation matches very well with the simulations.

### C. Simultaneous Localization and Communication

1) *Localization Performance*: In Fig. 4, we present the localization performance with the same setup in Fig. 3. From Fig. 4, it is clear that the first-order perturbation of the position estimation is accurate (the absolute value of the difference is decreasing with SNR.) in high SNR region since higher orders can be reasonably ignored. Comparatively, the directional beams with closer beam separation can improve position estimation performance, which agrees with the analytical results. This can be attributed to the channel parameter estimation performance improvements as shown in Fig. 3. To better illustrate the gap between the analytical and the numerical results in position estimation performance, we refer to the approximation made in (78), where the last three components are the second-order perturbations. Since  $\Delta\mu_l$  and  $\Delta\delta_l$  are correlated as indicated by (75) and (76), the mean and covariance of the second-order perturbations are not zero, leading to the gap shown in Fig. 4. This also indicates that a higher order perturbation analysis (for example, second order) is required for position estimation, which is left for future work.

2) *Achievable Rate*: Next, we evaluate the achievable rate performance of the system. The effective achievable rate is computed as in (9). In Fig. 5, we show the effective achievable rate performance in the following conditions: 1) perfect channel state information (CSI) knowledge, 2) estimated CSI with the proposed method. It is obvious that the proposed beamspace ESPRIT approach achieves near-optimal achievable rate performance. This indicates that the proposed schemes reconstruct the optimal CSI for communications, agreeing with the channel estimation performance validated in Fig. 6b. In addition, the effective achievable rate performance with directional beams ( $\pi/8$  beam separation) outperforms that with the DFT beams ( $\pi/4$  beam separation), which is attributed to high effective SNR with the closer beam separation. Together with the localization performance in Fig. 4, we conclude that the optimal spatial signal design for simultaneous localization and communications is required, which can be a future research topic.

### D. Performance Comparison to Existing Work

We now compare the estimation performance of the proposed method to existing work in [20], [21]. It is worth pointing out that the work in [20], [21] explores the ESPRIT approaches based on tensor decomposition, and has been applied to DFT beams and random beams for angular frequency estimations. We extend the tensor-based ESPRIT approaches in [20], [21] to arbitrary directional beams, and use it for channel parameter and position estimation. In the

proposed method, we have applied the spatial smoothing over frequency domain, which potentially utilize the frequency domain samples more efficiently. As a result, the delay estimation performance in the proposed method can be significantly improved. Because of the improved delay estimation, the average angular frequency estimation performance over all dimensions is significantly improved, as shown in Fig. 6a. With the estimated channel parameters, we can also reconstruct the high dimensional channel  $\mathcal{H}$ . It is clear from Fig. 6b that the proposed method achieves significantly improved channel estimation performance over the tensor decomposition based methods in [20], [21]. The channel parameter estimations can be used to infer user location, and it is quite obvious that the proposed method show much improved localization performance over the existing work. It is also worth pointing out that the directional beams with closer beam separation can significantly improve the estimation performance of the tensor-based ESPRIT approach. This is because in the tensor-based ESPRIT approach [20], [21], using closer beam separation can significantly improve the angle estimation for multipath components. On the other hand, in the proposed scheme, we have employed the spatial smoothing techniques, which has improved the delay solution for multipath components. As a result, the performance improvement gap of using the directional beams with closer beam separation over the DFT beams is not as much as the tensor-based methods.

As indicated in Section IV-E2, the proposed method enjoys low complexity, particularly in multi-path scenarios. This can be well demonstrated with the CPU running time of the program, as shown in Fig. 7. We generate multiple scatter points from the scatter region, and evaluate the run time of the proposed method and the tensor-based method in [20], [21]. It is obvious that when the number of multi-path components increases, the tensor-based method requires considerable computation time, which is attributed to the high complexity in CP decomposition algorithm for high order tensors. On the other hand, the proposed method utilizes the FFT/IFFT algorithms to obtain the signal subspace, and the complexity almost grows linearly to the number of multi-path components. The results indicate that the proposed beamspace ESPRIT method has great potential in real-time positioning applications.

## VII. CONCLUSION

In this paper, we have proposed a novel beamspace multi-dimensional ESPRIT method for simultaneous localization and communications. The proposed method employs spatial smoothing techniques over the frequency domain and can work with arbitrary beamforming and combining matrices used at transmitter and receiver sides. In addition, we have proposed a low-complexity method to obtain the signal subspace by using the properties of Hankel matrices. With the first-order perturbation analysis, we have successfully obtained the closed-form estimation performance of the proposed method. Through numerical simulations, we have shown that the proposed method achieves promising estimation performance with both DFT and directional beams used in the system, and the numerical results match well with the analytical results. Moreover, the

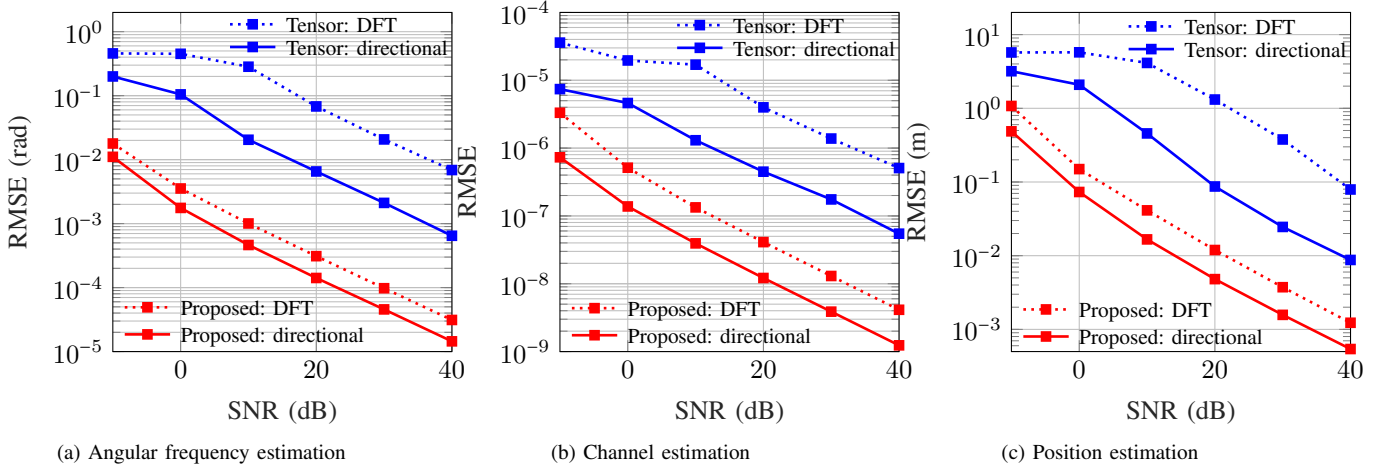


Fig. 6: Performance comparison: 1 LOS and 1 NLOS,  $N_P = 32$ , DFT beams and directional beams.

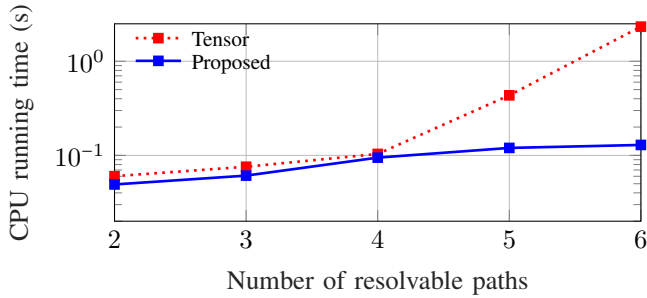


Fig. 7: Program running time performance.

directional beams with closer beam separation can further improve the estimation performance. We have also shown that the program running time of the proposed method outperforms existing tensor decomposition based ESPRIT method, especially in reasonable rich multi-path scenarios. Finally, we have investigated the achievable rate performance and shown that the proposed method achieves near-optimal achievable rate performance.

#### APPENDIX A FACTORIZATION OF $\mathbf{H}$

From (14) and (15), the  $\ell_5$ -th column of  $\mathbf{H}$  is given by

$$\begin{aligned} \mathbf{J}_{M_1, M_2, M_3, M_4, \ell_5} \mathbf{h}^{(b)} &= (\mathbf{I}_{M_1} \otimes \mathbf{I}_{M_2} \otimes \mathbf{I}_{M_3} \otimes \mathbf{I}_{M_4} \otimes \mathbf{J}_{\ell_5}) \\ &\quad \times (\mathbf{B}_1^{(N_1)} \circledast \mathbf{B}_2^{(N_2)} \circledast \dots \circledast \mathbf{B}_5^{(N_5)}) \boldsymbol{\gamma} \\ &= (\mathbf{B}_1^{(N_1)} \circledast \mathbf{B}_2^{(N_2)} \circledast \dots \circledast \mathbf{A}_5^{(K_5)}) \\ &\quad \times \text{Diag}(\boldsymbol{\omega}_5^{\ell_5-1}) \boldsymbol{\gamma}, \end{aligned}$$

where  $\boldsymbol{\omega}_5^\ell = [\exp(j\ell\omega_{1,5}), \exp(j\ell\omega_{2,5}), \dots, \exp(j\ell\omega_{L,5})]^\top$ . Therefore, we have

$$\begin{aligned} \mathbf{H} &= [\mathbf{P}\text{Diag}(\boldsymbol{\omega}_5^0) \boldsymbol{\gamma}, \mathbf{P}\text{Diag}(\boldsymbol{\omega}_5^1) \boldsymbol{\gamma}, \dots, \mathbf{P}\text{Diag}(\boldsymbol{\omega}_5^{L_5-1}) \boldsymbol{\gamma}] \\ &= \mathbf{P}\text{Diag}(\boldsymbol{\gamma}) [\boldsymbol{\omega}_5^0, \boldsymbol{\omega}_5^1, \dots, \boldsymbol{\omega}_5^{L_5-1}] \\ &= \mathbf{P}\text{Diag}(\boldsymbol{\gamma}) \mathbf{G}, \end{aligned}$$

where  $\mathbf{P}$  and  $\mathbf{G}$  are given in (17) and (18), respectively.

#### APPENDIX B PROOFS

##### A. Proof of Proposition 2

For  $n = 1, 2, 3, 4$ , using the properties of the Khatri-Rao products [28], we have

$$\begin{aligned} \check{\mathbf{J}}_{n,1} \mathbf{P} \boldsymbol{\Phi}_n &= (\mathbf{I}_{N_1} \otimes \dots \otimes \mathbf{L}_{n,1} \otimes \dots \otimes \mathbf{I}_{N_4} \otimes \mathbf{I}_{K_5}) \\ &\quad \times (\mathbf{B}_1^{(N_1)} \circledast \dots \circledast \mathbf{B}_n^{(N_n)} \circledast \dots \circledast \mathbf{B}_4^{(N_4)} \circledast \mathbf{A}_5^{(K_5)}) \boldsymbol{\Phi}_n \\ &= \mathbf{B}_1^{(N_1)} \circledast \dots \circledast \mathbf{L}_{n,1} \mathbf{B}_n^{(N_n)} \boldsymbol{\Phi}_n \circledast \dots \circledast \mathbf{B}_4^{(N_4)} \circledast \mathbf{A}_5^{(K_5)} \\ &= \mathbf{B}_1^{(N_1)} \circledast \dots \circledast \mathbf{L}_{n,2} \mathbf{B}_n^{(N_n)} \circledast \dots \circledast \mathbf{B}_4^{(N_4)} \circledast \mathbf{A}_5^{(K_5)} \\ &= \check{\mathbf{J}}_{n,2} \mathbf{P}, \end{aligned}$$

where the results  $\mathbf{L}_{n,1} \mathbf{B}_n^{(N_n)} \boldsymbol{\Phi}_n = \mathbf{L}_{n,2} \mathbf{B}_n^{(N_n)}$  in Proposition 1 is used in the above derivation. Following the similar process, we also have  $\check{\mathbf{J}}_{5,1} \mathbf{P} \boldsymbol{\Phi}_5 = \check{\mathbf{J}}_{5,2} \mathbf{P}$ .

##### B. Proof of Lemma 1

To begin with, we introduce the following results for the perturbation of signal subspace  $\mathbf{U}_s$ .

**Lemma 4.** Given the perturbed  $\tilde{\mathbf{H}}$  in (35), and the subspace decomposition as

$$\tilde{\mathbf{H}} = \tilde{\mathbf{U}}_s \tilde{\boldsymbol{\Sigma}}_s \tilde{\mathbf{V}}_s^H + \tilde{\mathbf{U}}_n \tilde{\boldsymbol{\Sigma}}_n \tilde{\mathbf{V}}_n^H,$$

the first-order approximation of the  $\Delta \mathbf{U}_s = \tilde{\mathbf{U}}_s - \mathbf{U}_s$  is given by

$$\Delta \mathbf{U}_s = \mathbf{U}_n \mathbf{U}_n^H \Delta \mathbf{H} \mathbf{V}_s \boldsymbol{\Sigma}_s^{-1} + \mathbf{U}_s \mathbf{R}, \quad (64)$$

where  $\mathbf{R}$  is an anti-Hermitian matrix that depends on  $\Delta \mathbf{H}$ .

*Proof.* The proof can be seen in [11].  $\square$

With  $\Delta \mathbf{U}_s$ , the first-order approximation of  $\Delta \boldsymbol{\Gamma}_n = \tilde{\boldsymbol{\Gamma}}_n - \boldsymbol{\Gamma}_n$  can be obtained as follows.

**Lemma 5.**  $\Delta \boldsymbol{\Gamma}_n$  is given by

$$\Delta \boldsymbol{\Gamma}_n = (\check{\mathbf{J}}_{n,1} \mathbf{U}_s)^\dagger (\check{\mathbf{J}}_{n,2} \Delta \mathbf{U}_s - \check{\mathbf{J}}_{n,1} \Delta \mathbf{U}_s \boldsymbol{\Gamma}_n). \quad (65)$$

*Proof.* Using the fact that  $\Delta(\mathbf{A}^\dagger) = -\mathbf{A}^\dagger \Delta \mathbf{A} \mathbf{A}^\dagger + (\mathbf{A}^\text{H} \mathbf{A})^{-1} \Delta \mathbf{A}^\text{H} (\mathbf{I} - \mathbf{A} \mathbf{A}^\dagger)$ , we find from (23) and using  $(\mathbf{I} - \check{\mathbf{J}}_{n,1} \mathbf{U}_s (\check{\mathbf{J}}_{n,1} \mathbf{U}_s)^\dagger) \check{\mathbf{J}}_{n,2} \mathbf{U}_s = \mathbf{0}$ , we obtain

$$\Delta \Gamma_n = \Delta(\check{\mathbf{J}}_{n,1} \mathbf{U}_s)^\dagger \check{\mathbf{J}}_{n,2} \mathbf{U}_s + (\check{\mathbf{J}}_{n,1} \mathbf{U}_s)^\dagger \check{\mathbf{J}}_{n,2} \Delta \mathbf{U}_s$$

from which (65) follows.  $\square$

Denote  $\mathbf{E} = [\mathbf{e}_1, \mathbf{e}_2, \dots, \mathbf{e}_L]$  and  $\mathbf{E}^{-1} = [\epsilon_1, \epsilon_2, \dots, \epsilon_L]^\text{T}$ . Then the first-order approximation of  $\Delta \Phi_{l,n} = \check{\Phi}_{l,n} - \Phi_{l,n}$  is given as follows.

**Lemma 6.**  $\Delta \Phi_{l,n}$  is given by

$$\Delta \Phi_{l,n} = \epsilon_l^\text{T} \Delta \Gamma_n \mathbf{e}_l. \quad (66)$$

*Proof.* From (26), we have

$$\begin{aligned} \Delta \Phi_n &= \mathbf{E}^{-1} \Delta \Gamma_n \mathbf{E} + \mathbf{E}^{-1} \Gamma_n \Delta \mathbf{E} - \mathbf{E}^{-1} \Delta \mathbf{E} \mathbf{E}^{-1} \Gamma_n \mathbf{E} \\ &= \mathbf{E}^{-1} \Delta \Gamma_n \mathbf{E} + \Phi_n \mathbf{E}^{-1} \Delta \mathbf{E} - \mathbf{E}^{-1} \Delta \mathbf{E} \Phi_n. \end{aligned} \quad (67)$$

We extract the diagonal element from the right hand side, and the last two terms are canceled, leading to the results in (66).  $\square$

In order to prove Lemma 1, we apply Lemma 4 to Lemmas 5–6. We define  $\mathbf{C} = \Delta \mathbf{H} \mathbf{V}_s \Sigma_s^{-1}$ , which allows us to write:

$$\begin{aligned} \Delta \Gamma_n &= (\check{\mathbf{J}}_{n,1} \mathbf{U}_s)^\dagger (\check{\mathbf{J}}_{n,2} \mathbf{C} - \check{\mathbf{J}}_{n,1} \mathbf{C} \Gamma_n) - \Gamma_n \mathbf{U}_s^\text{H} \mathbf{C} \\ &\quad + \mathbf{U}_s^\text{H} \mathbf{C} \Gamma_n + \Gamma_n \mathbf{R} - \mathbf{R} \Gamma_n. \end{aligned} \quad (68)$$

$$\Delta \Phi_{l,n} = \epsilon_l^\text{T} (\check{\mathbf{J}}_{n,1} \mathbf{U}_s)^\dagger (\check{\mathbf{J}}_{n,2} - \Phi_{l,n} \check{\mathbf{J}}_{n,1}) \mathbf{C} \mathbf{e}_l, \quad (69)$$

where  $\Gamma_n \mathbf{e}_l = \Phi_{l,n} \mathbf{e}_l$  and  $\epsilon_l \Gamma_n = \Phi_{l,n} \epsilon_l$  are used in the derivation. Finally, from (16) and (20), we have  $\mathbf{U}_s = \mathbf{P} \mathbf{E}^{-1}$ , and  $\Sigma_s \mathbf{V}_s^\text{H} = \mathbf{E} \text{Diag}(\gamma) \mathbf{G}^\text{T}$  leading to

$$\begin{aligned} \Delta \Phi_{l,n} &= \epsilon_l^\text{T} (\check{\mathbf{J}}_{n,1} \mathbf{P} \mathbf{E}^{-1})^\dagger (\check{\mathbf{J}}_{n,2} - \Phi_{l,n} \check{\mathbf{J}}_{n,1}) \Delta \mathbf{H} (\Sigma_s \mathbf{V}_s^\text{H})^\dagger \mathbf{e}_l \\ &= \frac{1}{\gamma_l} \mathbf{b}_l^\text{T} (\check{\mathbf{J}}_{n,1} \mathbf{P})^\dagger (\check{\mathbf{J}}_{n,2} - \Phi_{l,n} \check{\mathbf{J}}_{n,1}) \Delta \mathbf{H} (\mathbf{G}^\text{T})^\dagger \mathbf{b}_l, \end{aligned}$$

which is the result in (36).

### C. Proof of Proposition 3

We first present the following lemma.

**Lemma 7.** Given  $\mathbf{a} = [\mathbf{a}_{1,1,1,1}^\text{T}, \mathbf{a}_{1,1,1,2}^\text{T}, \dots, \mathbf{a}_{N_1, N_2, N_3, N_4}^\text{T}]^\text{T}$  where  $\mathbf{a}_{n_1, n_2, n_3, n_4} \in \mathbb{C}^{K_5 \times 1}$  and  $\mathbf{b} \in \mathbb{C}^{L_5 \times 1}$ , we have  $\mathbf{a}^\text{H} \Delta \mathbf{H} \mathbf{b}^* = \mathbf{c}^\text{H} \Delta \mathbf{h}$ , where  $\mathbf{c} = [\mathbf{c}_{1,1,1,1}^\text{T}, \mathbf{c}_{1,1,1,2}^\text{T}, \dots, \mathbf{c}_{N_1, N_2, N_3, N_4}^\text{T}]^\text{T}$  and  $\mathbf{c}_{n_1, n_2, n_3, n_4} \in \mathbb{C}^{M_5 \times 1}$  is the convolution of  $\mathbf{a}_{n_1, n_2, n_3, n_4}$  and  $\mathbf{b}$ .

*Proof.* Let  $\mathbf{y} = \Delta \mathbf{H} \mathbf{b}^*$ , where  $\mathbf{y} \in \mathbb{C}^{N_1 N_2 N_3 N_4 K_5 \times 1}$  is given by  $\mathbf{y} = [\mathbf{y}_{1,1,1,1}^\text{T}, \mathbf{y}_{1,1,1,2}^\text{T}, \dots, \mathbf{y}_{N_1, N_2, N_3, N_4}^\text{T}]^\text{T}$ , and  $\mathbf{y}_{n_1, n_2, n_3, n_4} \in \mathbb{C}^{K_5 \times 1}$ . Accordingly, we have  $\mathbf{y}_{n_1, n_2, n_3, n_4} = \Delta \mathbf{H}_{n_1, n_2, n_3, n_4} \mathbf{b}^*$ . As a result,

$$\begin{aligned} \mathbf{a}^\text{H} \Delta \mathbf{H} \mathbf{b}^* &= \sum_{n_1=1}^{N_1} \sum_{n_2=1}^{N_2} \sum_{n_3=1}^{N_3} \sum_{n_4=1}^{N_4} \sum_{m_5=1}^{M_5} \Delta \mathbf{h}_{n_1, n_2, n_3, n_4, m_5} \\ &\quad \underbrace{\sum_{\ell_5=1}^{L_5} a_{n_1, n_2, n_3, n_4, m_5+1-\ell_5}^* \mathbf{b}_{\ell_5}^*}_{\mathbf{c}_{n_1, n_2, n_3, n_4, m_5}^*} \end{aligned}$$

which shows that  $\mathbf{a}^\text{H} \Delta \mathbf{H} \mathbf{b}^* = \mathbf{c}^\text{H} \Delta \mathbf{h}$ .  $\square$

With the results in Lemma 1, we obtain the results in (41) by applying the results in Lemma 7.

### D. Proof of Lemma 2

With the relationship between the angular frequencies and channel parameters, we establish the following first-order perturbations:  $\Delta \omega_{l,1} = \pi \cos(\phi_{az}^l) \sin(\phi_{el}^l) \Delta \phi_{az}^l + \pi \sin(\phi_{az}^l) \cos(\phi_{el}^l) \Delta \phi_{el}^l$ ,  $\Delta \omega_{l,2} = -\pi \sin(\phi_{el}^l) \Delta \phi_{el}^l$ ,  $\Delta \omega_{l,3} = \pi \cos(\theta_{az}^l) \sin(\theta_{el}^l) \Delta \theta_{az}^l + \pi \sin(\theta_{az}^l) \cos(\theta_{el}^l) \Delta \theta_{el}^l$ ,  $\Delta \omega_{l,4} = -\pi \sin(\theta_{el}^l) \Delta \theta_{el}^l$ , and  $\Delta \omega_{l,5} = -2\pi \Delta f \Delta \tau_l$ . Using the results in (42), it is straightforward to obtain the results in (43)–(45).

Obtaining (46) is more involved. First of all, with  $\Delta \omega_{l,n}$ , we have  $\Delta(\exp(jm_n \omega_{l,n})) = jm_n \exp(jm_n \omega_{l,n}) \Delta \omega_{l,n}$ , so that the first-order perturbation of  $\mathbf{A}_n^{(M_n)}$  is given by  $\Delta \mathbf{A}_n^{(M_n)} = j \text{Diag}(\mathbf{m}_n) \mathbf{A}_n^{(M_n)} \text{Diag}(\Delta \omega_n)$ , where  $\mathbf{m}_n = [0, 1, \dots, M_n - 1]^\text{T}$  and  $\Delta \omega_n = [\Delta \omega_{1,n}, \Delta \omega_{2,n}, \dots, \Delta \omega_{L,n}]^\text{T} = \mathcal{J}\{\mathbf{V}_n^\text{H} \Delta \mathbf{h}\}$ . From this, we see that the first-order perturbation of  $\mathbf{B}_n^{(N_n)}$  is given by  $\Delta \mathbf{B}_n^{(N_n)} = \mathbf{T}_n^\text{H} \Delta \mathbf{A}_n^{(M_n)} = \check{\mathbf{T}}_n^\text{H} \mathbf{A}_n^{(M_n)} \odot \Delta \omega_n^\text{T}$  where  $\mathbf{T}_n = -j \text{Diag}(\mathbf{m}_n) \mathbf{T}_n$ . From (28), we derive the first-order perturbation  $\Delta \mathbf{B}$  as  $\Delta \mathbf{B} = \sum_{n=1}^5 \check{\mathbf{B}}_n \odot \Delta \omega_n^\text{T}$ , where

$$\check{\mathbf{B}}_n = \mathbf{B}_1^{(N_1)} \odot \dots \odot \check{\mathbf{T}}_n^\text{H} \mathbf{A}_n^{(M_n)} \odot \dots \odot \mathbf{B}_5^{(N_5)}. \quad (70)$$

From the proof of Lemma 5, we recall that  $\Delta(\mathbf{B}^\dagger) = -\mathbf{B}^\dagger \Delta \mathbf{B} \mathbf{B}^\dagger + (\mathbf{B}^\text{H} \mathbf{B})^{-1} \Delta \mathbf{B}^\text{H} (\mathbf{I} - \mathbf{B} \mathbf{B}^\dagger)$ . Secondly, we note that the estimate of the channel gain  $\gamma$  is given as

$$\hat{\gamma} = \gamma + \mathbf{B}^\dagger \Delta \mathbf{h} + \Delta(\mathbf{B}^\dagger) \mathbf{B} \gamma + \Delta(\mathbf{B}^\dagger) \Delta \mathbf{h}, \quad (71)$$

which indicates that the first-order perturbation of the channel gain estimation is

$$\begin{aligned} \Delta \gamma &= \mathbf{B}^\dagger \Delta \mathbf{h} + \Delta(\mathbf{B}^\dagger) \mathbf{B} \gamma \\ &= \mathbf{B}^\dagger \Delta \mathbf{h} - \sum_{n=1}^5 \Upsilon_n \mathcal{J}\{\mathbf{V}_n^\text{H} \Delta \mathbf{h}\}. \end{aligned} \quad (72)$$

### E. Proof of Lemma 3

To begin with, we have the first-order approximations of  $\Delta \mathbf{f}_{\text{T},l}$  and  $\Delta \mathbf{f}_{\text{R},l}$  as  $\Delta \mathbf{f}_{\text{T},l} = \Omega_{\text{T},l} [\Delta \phi_{az}^l, \Delta \phi_{el}^l]^\text{T}$  and  $\Delta \mathbf{f}_{\text{R},l} = \Omega_{\text{R},l} [\Delta \theta_{az}^l, \Delta \theta_{el}^l]^\text{T}$ , respectively, where  $\Omega_{\text{T},l} \in \mathbb{R}^{3 \times 2}$  and  $\Omega_{\text{R},l} \in \mathbb{R}^{3 \times 2}$  are given by

$$\Omega_{\text{T},l} = \begin{bmatrix} -\sin(\phi_{az}^l) \sin(\phi_{el}^l) & \cos(\phi_{az}^l) \cos(\phi_{el}^l) \\ \cos(\phi_{az}^l) \sin(\phi_{el}^l) & \sin(\phi_{az}^l) \cos(\phi_{el}^l) \\ 0 & -\sin(\phi_{el}^l) \end{bmatrix}, \quad (73)$$

$$\Omega_{\text{R},l} = \begin{bmatrix} -\sin(\theta_{az}^l) \sin(\theta_{el}^l) & \cos(\theta_{az}^l) \cos(\theta_{el}^l) \\ \cos(\theta_{az}^l) \sin(\theta_{el}^l) & \sin(\theta_{az}^l) \cos(\theta_{el}^l) \\ 0 & -\sin(\theta_{el}^l) \end{bmatrix}. \quad (74)$$

As a result, the first-order approximations of  $\Delta \delta_l$  and  $\Delta \mu_l$  are obtained as

$$\Delta \delta_l = -c [\tau_l \Omega_{\text{R},l}, \mathbf{f}_{\text{R},l}] [\Delta \theta_{az}^l, \Delta \theta_{el}^l, \Delta \tau_l]^\text{T}, \quad (75)$$

$$\begin{aligned} \Delta \mu_l &= c [\tau_l \Omega_{\text{T},l}, \tau_l \Omega_{\text{R},l}, (\mathbf{f}_{\text{T},l} + \mathbf{f}_{\text{R},l})] \\ &\quad [\Delta \phi_{az}^l, \Delta \phi_{el}^l, \Delta \theta_{az}^l, \Delta \theta_{el}^l, \Delta \tau_l]^\text{T}. \end{aligned} \quad (76)$$

Since  $C_l = (\mathbf{I} - \boldsymbol{\mu}_l \boldsymbol{\mu}_l^T / \|\boldsymbol{\mu}_l\|^2)$ ,  $\Delta C_l$  can be given as<sup>4</sup>

$$\begin{aligned} \Delta C_l = & 2(\boldsymbol{\mu}_l^T \boldsymbol{\mu}_l)^{-2} (\boldsymbol{\mu}_l^T \Delta \boldsymbol{\mu}_l) \boldsymbol{\mu}_l \boldsymbol{\mu}_l^T \\ & - (\boldsymbol{\mu}_l^T \boldsymbol{\mu}_l)^{-1} (\Delta \boldsymbol{\mu}_l \boldsymbol{\mu}_l^T + \boldsymbol{\mu}_l \Delta \boldsymbol{\mu}_l^T). \end{aligned} \quad (77)$$

According to (7), and define  $\mathbf{C} = \sum_{l=1}^L C_l$ , we have

$$\begin{aligned} \hat{\mathbf{p}}_R &= \left( \sum_{l=1}^L C_l + \Delta C_l \right)^{-1} \sum_{l=1}^L (C_l + \Delta C_l) (\boldsymbol{\delta}_l + \Delta \boldsymbol{\delta}_l) \\ &\approx \mathbf{p}_R + \mathbf{C}^{-1} \sum_{l=1}^L \Delta C_l (\boldsymbol{\delta}_l - \mathbf{p}_R) + \mathbf{C}^{-1} \sum_{l=1}^L C_l \Delta \boldsymbol{\delta}_l \\ &+ \mathbf{C}^{-1} \sum_{l=1}^L \Delta C_l \Delta \boldsymbol{\delta}_l - \mathbf{C}^{-1} \sum_{l=1}^L \Delta C_l \mathbf{C}^{-1} \sum_{l=1}^L C_l \Delta \boldsymbol{\delta}_l \\ &+ \mathbf{C}^{-1} \sum_{l=1}^L \Delta C_l \mathbf{C}^{-1} \sum_{l=1}^L \Delta C_l (\mathbf{p}_R - \boldsymbol{\delta}_l), \end{aligned} \quad (78)$$

where higher order approximation is omitted. Therefore, the first-order perturbation of the position estimate, i.e.,  $\Delta \mathbf{p}_R = \hat{\mathbf{p}}_R - \mathbf{p}_R$ , can be obtained as

$$\begin{aligned} \Delta \mathbf{p}_R &= \mathbf{C}^{-1} \sum_{l=1}^L \Delta C_l (\boldsymbol{\delta}_l - \mathbf{p}_R) + \mathbf{C}^{-1} \sum_{l=1}^L C_l \Delta \boldsymbol{\delta}_l \\ &= \mathbf{C}^{-1} \sum_{l=1}^L \check{C}_l \Delta \boldsymbol{\mu}_l + C_l \Delta \boldsymbol{\delta}_l, \end{aligned} \quad (79)$$

where  $\check{C}_l \in \mathbb{R}^{3 \times 3}$  is given by

$$\begin{aligned} \check{C}_l &= \frac{2\boldsymbol{\mu}_l^T (\boldsymbol{\delta}_l - \mathbf{p}_R) \boldsymbol{\mu}_l \boldsymbol{\mu}_l^T}{\|\boldsymbol{\mu}_l\|^4} \\ &- \frac{\boldsymbol{\mu}_l^T (\boldsymbol{\delta}_l - \mathbf{p}_R) \mathbf{I} + \boldsymbol{\mu}_l (\boldsymbol{\delta}_l - \mathbf{p}_R)^T}{\|\boldsymbol{\mu}_l\|^2}. \end{aligned} \quad (80)$$

Substituting the results in (75) and (76) to (79), we arrive at

$$\begin{aligned} \Delta \mathbf{p}_R &= \sum_{l=1}^L \check{D}_l [\Delta \theta_{az}^l, \Delta \theta_{el}^l, \Delta \tau_l]^T \\ &+ \check{E}_l [\Delta \phi_{az}^l, \Delta \phi_{el}^l, \Delta \theta_{az}^l, \Delta \theta_{el}^l, \Delta \tau_l]^T, \end{aligned} \quad (81)$$

where  $\check{D}_l \in \mathbb{R}^{3 \times 3}$  and  $\check{E}_l \in \mathbb{R}^{3 \times 5}$

$$\check{D}_l = -c \left( \sum_{\ell=1}^L C_\ell \right)^{-1} C_l [\tau_l \boldsymbol{\Omega}_{R,l}, \mathbf{f}_{R,l}], \quad (82)$$

$$\check{E}_l = c \left( \sum_{\ell=1}^L C_\ell \right)^{-1} \check{C}_l [\tau_l \boldsymbol{\Omega}_{T,l}, \tau_l \boldsymbol{\Omega}_{R,l}, (\mathbf{f}_{T,l} + \mathbf{f}_{R,l})]. \quad (83)$$

With the results in Lemma 2, we derive the results in (59).

#### ACKNOWLEDGMENT

The authors would like to thank the editors and autonomous reviewers for your time and effort in handling the review of our paper.

<sup>4</sup>We omit  $\iota_l$ .

#### REFERENCES

- [1] G. Destino and H. Wymeersch, "On the trade-off between positioning and data rate for mm-wave communication," in *2017 IEEE International Conference on Communications Workshops (ICC Workshops)*. IEEE, 2017, pp. 797–802.
- [2] R. Koirala, B. Denis, B. Uguen, D. Dardari, and H. Wymeersch, "Localization and throughput trade-off in a multi-user multi-carrier mm-wave system," *IEEE Access*, vol. 7, pp. 167 099–167 112, 2019.
- [3] R. Di Taranto, S. Muppirisetty, R. Raulefs, D. Slock, T. Svensson, and H. Wymeersch, "Location-aware communications for 5g networks: How location information can improve scalability, latency, and robustness of 5g," *IEEE Signal Processing Magazine*, vol. 31, no. 6, pp. 102–112, 2014.
- [4] S. Jayaprakasam, X. Ma, J. W. Choi, and S. Kim, "Robust beam-tracking for mmwave mobile communications," *IEEE Communications Letters*, vol. 21, no. 12, pp. 2654–2657, 2017.
- [5] A. Alkhatieb, O. El Ayach, G. Leus, and R. W. Heath, "Channel estimation and hybrid precoding for millimeter wave cellular systems," *IEEE journal of selected topics in signal processing*, vol. 8, no. 5, pp. 831–846, 2014.
- [6] Y. Ge, F. Wen, H. Kim, M. Zhu, F. Jiang, S. Kim, L. Svensson, and H. Wymeersch, "5G SLAM Using the Clustering and Assignment Approach with Diffuse Multipath," *Sensors*, vol. 20, no. 16, p. 4656, Aug. 2020.
- [7] A. Richter, "Estimation of radio channel parameters: Models and algorithms," Ph.D. dissertation, TU Ilmenau, 2005.
- [8] L. Huang, Y. Wu, H.-C. So, Y. Zhang, and L. Huang, "Multidimensional sinusoidal frequency estimation using subspace and projection separation approaches," *IEEE Transactions on Signal Processing*, vol. 60, no. 10, pp. 5536–5543, 2012.
- [9] J. Lee, G.-T. Gil, and Y. H. Lee, "Channel estimation via orthogonal matching pursuit for hybrid mimo systems in millimeter wave communications," *IEEE Transactions on Communications*, vol. 64, no. 6, pp. 2370–2386, 2016.
- [10] Y. Tsai, L. Zheng, and X. Wang, "Millimeter-wave beamformed full-dimensional mimo channel estimation based on atomic norm minimization," *IEEE Transactions on Communications*, vol. 66, no. 12, pp. 6150–6163, 2018.
- [11] S. Sahnoun, K. Usevich, and P. Comon, "Multidimensional ESPRIT for Damped and Undamped Signals: Algorithm, Computations, and Perturbation Analysis," *IEEE Transactions on Signal Processing*, vol. 65, no. 22, pp. 5897–5910, Nov. 2017.
- [12] A. B. Gershman, M. RübSamen, and M. Pesavento, "One-and two-dimensional direction-of-arrival estimation: An overview of search-free techniques," *Signal Processing*, vol. 90, no. 5, pp. 1338–1349, 2010.
- [13] R. Roy and T. Kailath, "ESPRIT-Estimation of Signal Parameters via Rotational Invariance Techniques," *IEEE Transactions on Acoustics, Speech, and Signal Processing*, vol. 37, no. 7, pp. 984–995, Jul. 1989.
- [14] G. Xu, S. Silverstein, R. Roy, and T. Kailath, "Beamspace esprit," *IEEE Trans. Signal Process.*, vol. 42, no. 2, pp. 349–356, Feb. 1994.
- [15] J. Zhang, D. Rakhimov, and M. Haardt, "Gridless channel estimation for hybrid mmwave MIMO systems via tensor-ESPRIT algorithms in DFT beamspace," *IEEE Journal of Selected Topics in Signal Processing*, vol. 15, no. 3, pp. 816–831, 2021.
- [16] F. Wen, H. Wymeersch, B. Peng, W. P. Tay, H. C. So, and D. Yang, "A survey on 5G massive MIMO localization," *Digital Signal Processing*, vol. 94, pp. 21–28, 2019.
- [17] M. Haardt, F. Roemer, and G. Del Galdo, "Higher-order SVD-based subspace estimation to improve the parameter estimation accuracy in multidimensional harmonic retrieval problems," *IEEE Transactions on Signal Processing*, vol. 56, no. 7, pp. 3198–3213, 2008.
- [18] R. W. Heath, N. González-Prelcic, S. Rangan, W. Roh, and A. M. Sayeed, "An overview of signal processing techniques for millimeter wave MIMO systems," *IEEE Journal of Selected Topics in Signal Processing*, vol. 10, no. 3, pp. 436–453, 2016.
- [19] J. Zhang and M. Haardt, "Channel estimation and training design for hybrid multi-carrier mmwave massive MIMO systems: The beamspace esprit approach," in *IEEE EUSIPCO*, Kos, 2017.
- [20] F. Wen, N. Garcia, J. Kulmer, K. Witrisal, and H. Wymeersch, "Tensor decomposition based beamspace ESPRIT for millimeter wave mimo channel estimation," in *IEEE GLOBECOM*, Abu Dhabi, United Arab Emirates, 2018.
- [21] F. Wen, H. C. So, and H. Wymeersch, "Tensor decomposition-based beamspace ESPRIT algorithm for multidimensional harmonic retrieval," in *IEEE ICASSP*, Barcelona, Spain, 2020.

- [22] F. Wen, J. Kulmer, K. Witrissal, and H. Wymeersch, "5G positioning and mapping with diffuse multipath," *IEEE Transactions on Wireless Communications*, vol. 20, no. 2, pp. 1164–1174, 2021.
- [23] H. Wymeersch, "A simple method for 5G positioning and synchronization without line-of-sight," *arXiv:1812.05417*, 2018.
- [24] O. Raeesi, A. Gokceoglu, Y. Zou, E. Björnson, and M. Valkama, "Performance analysis of multi-user massive MIMO downlink under channel non-reciprocity and imperfect CSI," *IEEE Trans. Commun.*, vol. 66, no. 6, pp. 2456–2471, Jun. 2018.
- [25] T. G. Kolda and B. W. Bader, "Tensor decompositions and applications," *SIAM Review*, vol. 51, no. 3, pp. 455–500, Aug. 2009.
- [26] F. Jiang, Y. Ge, M. Zhu, and H. Wymeersch, "High-dimensional channel estimation for simultaneous localization and communications," in *2021 IEEE WCNC*, Nanjing, China, 2021.
- [27] L. Lu, W. Xu, and S. Qiao, "A Fast SVD for Multilevel Block Hankel Matrices with Minimal Memory Storage," *Linear Algebra and its Applications*, vol. 69, no. 4, pp. 875–891, Oct. 2015.
- [28] J. Liu and X. Liu, "An Eigenvector-based Approach for Multidimensional Frequency Estimation with Improved Identifiability," *IEEE Transactions on Signal Processing*, vol. 54, no. 12, pp. 4543–4556, Dec. 2006.
- [29] J. Liu, X. Liu, and X. Ma, "Multidimensional Frequency Estimation with Finite Snapshots in the Presence of Identical Frequencies," *IEEE Transactions on Signal Processing*, vol. 55, no. 11, pp. 5179–5194, Nov. 2007.
- [30] M. Sørensen and L. Lathauwer, "Multidimensional harmonic retrieval via coupled canonical polyadic decomposition—Part I: Model and identifiability," *IEEE Transactions on Signal Processing*, vol. 65, no. 2, pp. 517–527, Jan. 2016.

# SUPPLEMENTARY MATERIAL

## APPENDIX C PROOFS OF LEMMAS

### A. Proof of Lemma 1

To begin with, we introduce the following results for the perturbation of signal subspace  $U_s$ .

**Lemma 8.** *Given the perturbed  $\tilde{H}$  in (35), and the subspace decomposition as*

$$\tilde{H} = \tilde{U}_s \tilde{\Sigma}_s \tilde{V}_s^H + \tilde{U}_n \tilde{\Sigma}_n \tilde{V}_n^H,$$

the first-order approximation of the  $\Delta U_s = \tilde{U}_s - U_s$  is given by

$$\Delta U_s = U_n U_n^H \Delta H V_s \Sigma_s^{-1} + U_s R, \quad (84)$$

where  $R$  is an antihermitian matrix that depends on  $\Delta H$ .

*Proof.* The proof can be seen in [11].  $\square$

With  $\Delta U_s$ , the first-order approximation of  $\Delta \Gamma_n = \tilde{\Gamma}_n - \Gamma_n$  can be obtained as follows.

**Lemma 9.**  $\Delta \Gamma_n$  is given by

$$\Delta \Gamma_n = (\check{J}_{n,1} U_s)^\dagger (\check{J}_{n,2} \Delta U_s - \check{J}_{n,1} \Delta U_s \Gamma_n). \quad (85)$$

*Proof.* Using  $\Delta(T^{-1}) = -T^{-1} \Delta T T^{-1}$ , the perturbation of the inverse,  $\Delta((A^H A)^{-1})$  is given by

$$\begin{aligned} \Delta((A^H A)^{-1}) &= -(A^H A)^{-1} \Delta(A^H A) (A^H A)^{-1} \\ &= -(A^H A)^{-1} \Delta A^H A (A^H A)^{-1} \\ &\quad - (A^H A)^{-1} A^H \Delta A (A^H A)^{-1}. \end{aligned} \quad (86)$$

In addition,

$$\begin{aligned} \Delta(A^\dagger) &= -(A^H A)^{-1} \Delta A^H A (A^H A)^{-1} A^H \\ &\quad - (A^H A)^{-1} A^H \Delta A (A^H A)^{-1} A^H \\ &\quad + (A^H A)^{-1} \Delta A^H \\ &= -A^\dagger \Delta A A^\dagger + (A^H A)^{-1} \Delta A^H (I - A A^\dagger). \end{aligned} \quad (87)$$

From (23), we have

$$\begin{aligned} \Delta \Gamma_n &= \Delta(\check{J}_{n,1} U_s)^\dagger \check{J}_{n,2} U_s + (\check{J}_{n,1} U_s)^\dagger \check{J}_{n,2} \Delta U_s \\ &= (\check{J}_{n,1} U_s)^\dagger (\check{J}_{n,2} \Delta U_s - \check{J}_{n,1} \Delta U_s \Gamma_n). \end{aligned} \quad (88)$$

In the above derivation, the following equality is used.

$$(I - \check{J}_{n,1} U_s (\check{J}_{n,1} U_s)^\dagger) \check{J}_{n,2} U_s = 0.$$

$\square$

Denote  $E = [e_1, e_2, \dots, e_L]$  and  $E^{-1} = [\epsilon_1, \epsilon_2, \dots, \epsilon_L]^T$ . Then the first-order approximation of  $\Delta \Phi_{l,n} = \tilde{\Phi}_{l,n} - \Phi_{l,n}$  is given as follows.

**Lemma 10.**  $\Delta \Phi_{l,n}$  is given by

$$\Delta \Phi_{l,n} = \epsilon_l^T \Delta \Gamma_n e_l. \quad (89)$$

*Proof.* From (26), we have

$$\begin{aligned} \Delta \Phi_n &= E^{-1} \Delta \Gamma_n E + E^{-1} \Gamma_n \Delta E - E^{-1} \Delta E E^{-1} \Gamma_n E \\ &= E^{-1} \Delta \Gamma_n E + \Phi_n E^{-1} \Delta E - E^{-1} \Delta E \Phi_n. \end{aligned} \quad (90)$$

We extract the diagonal element from the right hand side, and the last two terms are canceled, leading to the results in (89).  $\square$

We are now able to apply the results in Lemma 8 and Lemma 9 to (89). For simplicity, we define  $C = \Delta H V_s \Sigma_s^{-1}$ . Using the results in (84), we then have  $\Delta \Gamma_n$  as

$$\begin{aligned} \Delta \Gamma_n &= (\check{J}_{n,1} U_s)^\dagger (\check{J}_{n,2} (I - U_s U_s^H) C - \check{J}_{n,1} (I - U_s U_s^H) C \Gamma_n) \\ &\quad + (\check{J}_{n,1} U_s)^\dagger (\check{J}_{n,2} U_s R - \check{J}_{n,1} U_s R \Gamma_n) \\ &= (\check{J}_{n,1} U_s)^\dagger (\check{J}_{n,2} C - \check{J}_{n,1} C \Gamma_n) - \Gamma_n U_s^H C \\ &\quad + U_s^H C \Gamma_n + \Gamma_n R - R \Gamma_n. \end{aligned} \quad (91)$$

With the result in (89),  $\Delta \Phi_{l,n}$  is further obtained as

$$\Delta \Phi_{l,n} = \epsilon_l^T (\check{J}_{n,1} U_s)^\dagger (\check{J}_{n,2} - \Phi_{l,n} \check{J}_{n,1}) C e_l, \quad (92)$$

where  $\Gamma_n e_l = \Phi_{l,n} e_l$  and  $\epsilon_l \Gamma_n = \Phi_{l,n} \epsilon_l$  are used in the derivation.

In addition, from (20) and (??), we have  $U_s = P E^{-1}$ , and  $\Sigma_s V_s^H = E \text{Diag}(\gamma) G^T$ . With these results,  $\Delta \Phi_{l,n}$  is rewritten as

$$\begin{aligned} \Delta \Phi_{l,n} &= \epsilon_l^T (\check{J}_{n,1} P E^{-1})^\dagger (\check{J}_{n,2} - \Phi_{l,n} \check{J}_{n,1}) \Delta H (\Sigma_s V_s^H)^\dagger e_l \\ &= \epsilon_l^T E (\check{J}_{n,1} P)^\dagger (\check{J}_{n,2} - \Phi_{l,n} \check{J}_{n,1}) \Delta H (G^T)^\dagger \\ &\quad (\text{Diag}(\gamma))^{-1} E^{-1} e_l \\ &= \frac{1}{\gamma_l} b_l^T (\check{J}_{n,1} P)^\dagger (\check{J}_{n,2} - \Phi_{l,n} \check{J}_{n,1}) \Delta H (G^T)^\dagger b_l, \end{aligned} \quad (93)$$

which is the result in (36).

### B. Proof of Proposition 3

To begin with, we have the following results.

**Lemma 11.** *Given*

$$\mathbf{a} = [\mathbf{a}_{1,1,1,1}^T, \mathbf{a}_{1,1,1,2}^T, \dots, \mathbf{a}_{1,1,1,N_4}^T, \mathbf{a}_{1,1,2,1}^T, \dots, \mathbf{a}_{N_1, N_2, N_3, N_4}^T]^T,$$

where  $\mathbf{a}_{n_1, n_2, n_3, n_4} \in \mathbb{C}^{K_5 \times 1}$  and  $\mathbf{b} \in \mathbb{C}^{L_5 \times 1}$ , we have

$$\mathbf{a}^H \Delta H \mathbf{b}^* = \mathbf{c}^H \Delta \mathbf{h}, \quad (94)$$

where

$$\mathbf{c} = [\mathbf{c}_{1,1,1,1}^T, \mathbf{c}_{1,1,1,2}^T, \dots, \mathbf{c}_{1,1,1,N_4}^T, \mathbf{c}_{1,1,2,1}^T, \dots, \mathbf{c}_{N_1, N_2, N_3, N_4}^T]^T,$$

and  $\mathbf{c}_{n_1, n_2, n_3, n_4} \in \mathbb{C}^{M_5 \times 1}$  is the convolution of  $\mathbf{a}_{n_1, n_2, n_3, n_4}$  and  $\mathbf{b}$ .

*Proof.* Let  $\mathbf{y} = \Delta H \mathbf{b}^*$ , where  $\mathbf{y} \in \mathbb{C}^{N_1 N_2 N_3 N_4 K_5 \times 1}$  is given by

$$\mathbf{y} = [\mathbf{y}_{1,1,1,1}^T, \mathbf{y}_{1,1,1,2}^T, \dots, \mathbf{y}_{1,1,1,N_4}^T, \mathbf{y}_{1,1,2,1}^T, \dots, \mathbf{y}_{N_1, N_2, N_3, N_4}^T]^T,$$

and  $\mathbf{y}_{n_1, n_2, n_3, n_4} \in \mathbb{C}^{K_5 \times 1}$ . Accordingly, we have

$$\mathbf{y}_{n_1, n_2, n_3, n_4} = \Delta H_{n_1, n_2, n_3, n_4} \mathbf{b}^*.$$

As a result, the left hand side of (94) is computed as

$$\begin{aligned}
\mathbf{a}^H \Delta \mathbf{H} \mathbf{b}^* &= \sum_{n_1=1}^{N_1} \sum_{n_2=1}^{N_2} \sum_{n_3=1}^{N_3} \sum_{n_4=1}^{N_4} \mathbf{a}_{n_1, n_2, n_3, n_4}^H \mathbf{y}_{n_1, n_2, n_3, n_4} \\
&= \sum_{n_1=1}^{N_1} \sum_{n_2=1}^{N_2} \sum_{n_3=1}^{N_3} \sum_{n_4=1}^{N_4} \sum_{k_5=1}^{K_5} a_{n_1, n_2, n_3, n_4, k_5}^* \\
&\quad \cdot \sum_{\ell_5=1}^{L_5} \Delta h_{n_1, n_2, n_3, n_4, k_5 + \ell_5 - 1} b_{\ell_5}^* \\
&= \sum_{n_1=1}^{N_1} \sum_{n_2=1}^{N_2} \sum_{n_3=1}^{N_3} \sum_{n_4=1}^{N_4} \sum_{m_5=1}^{M_5} \Delta h_{n_1, n_2, n_3, n_4, m_5} \\
&\quad \underbrace{\sum_{\ell_5=1}^{L_5} a_{n_1, n_2, n_3, n_4, m_5 + 1 - \ell_5}^* b_{\ell_5}^*}_{c_{n_1, n_2, n_3, n_4, m_5}^*} \\
&= \mathbf{c}^H \Delta \mathbf{h}, \tag{95}
\end{aligned}$$

which complete the proof.  $\square$

With the results in Lemma 11, we directly arrive at (41).

### C. Proof of Lemma 2

With the relationship between the angular frequencies and channel parameters, we establish the following first-order perturbation:

$$\begin{aligned}
\Delta \omega_{l,1} &= \pi \cos(\phi_{az}^l) \sin(\phi_{el}^l) \Delta \phi_{az}^l \\
&\quad + \pi \sin(\phi_{az}^l) \cos(\phi_{el}^l) \Delta \phi_{el}^l, \\
\Delta \omega_{l,2} &= -\pi \sin(\phi_{el}^l) \Delta \phi_{el}^l, \\
\Delta \omega_{l,3} &= \pi \cos(\theta_{az}^l) \sin(\theta_{el}^l) \Delta \theta_{az}^l \\
&\quad + \pi \sin(\theta_{az}^l) \cos(\theta_{el}^l) \Delta \theta_{el}^l, \\
\Delta \omega_{l,4} &= -\pi \sin(\theta_{el}^l) \Delta \theta_{el}^l, \\
\Delta \omega_{l,5} &= -2\pi \Delta f \Delta \tau_l.
\end{aligned}$$

Using the results in (42), it is straightforward to obtain the results in (43)-(45).

In addition, with  $\Delta \omega_{l,n}$ , we have

$$\Delta(\exp(jm_n \omega_{l,n})) = jm_n \exp(jm_n \omega_{l,n}) \Delta \omega_{l,n}.$$

Therefore, the first-order perturbation of  $\mathbf{A}_n^{(M_n)}$  is given by

$$\Delta \mathbf{A}_n^{(M_n)} = j \text{Diag}(\mathbf{m}_n) \mathbf{A}_n^{(M_n)} \text{Diag}(\Delta \boldsymbol{\omega}_n). \tag{96}$$

where  $\mathbf{m}_n = [0, 1, \dots, M_n - 1]^T$  and  $\Delta \boldsymbol{\omega}_n = [\Delta \omega_{1,n}, \Delta \omega_{2,n}, \dots, \Delta \omega_{L,n}]^T = \mathcal{J}\{\mathbf{V}_n^H \Delta \mathbf{h}\}$ .

The first-order perturbation of  $\mathbf{B}_n^{(N_n)}$  is given by

$$\Delta \mathbf{B}_n^{(N_n)} = \mathbf{T}_n^H \Delta \mathbf{A}_n^{(M_n)} = \check{\mathbf{T}}_n^H \mathbf{A}_n^{(M_n)} \odot \Delta \boldsymbol{\omega}_n^T, \tag{97}$$

where

$$\check{\mathbf{T}}_n = -j \text{Diag}(\mathbf{m}_n) \mathbf{T}_n.$$

From (28), we derive the first-order perturbation  $\Delta \mathbf{B}$  as

$$\Delta \mathbf{B} = \sum_{n=1}^5 \check{\mathbf{B}}_n \odot \Delta \boldsymbol{\omega}_n^T, \tag{98}$$

where

$$\check{\mathbf{B}}_n = \mathbf{B}_1^{(N_1)} \odot \dots \odot \check{\mathbf{T}}_n^H \mathbf{A}_n^{(M_n)} \odot \dots \odot \mathbf{B}_5^{(N_5)}. \tag{99}$$

According to (87), we have the perturbation  $\Delta(\mathbf{B}^\dagger)$  as

$$\Delta(\mathbf{B}^\dagger) = -\mathbf{B}^\dagger \Delta \mathbf{B} \mathbf{B}^\dagger + (\mathbf{B}^H \mathbf{B})^{-1} \Delta \mathbf{B}^H (\mathbf{I} - \mathbf{B} \mathbf{B}^\dagger). \tag{100}$$

As a result, the estimate of the channel gain  $\gamma$  is given as

$$\begin{aligned}
\hat{\gamma} &= (\mathbf{B}^\dagger + \Delta(\mathbf{B}^\dagger)) (\mathbf{B} \gamma + \Delta \mathbf{h}) \\
&= \gamma + \mathbf{B}^\dagger \Delta \mathbf{h} + \Delta(\mathbf{B}^\dagger) \mathbf{B} \gamma + \Delta(\mathbf{B}^\dagger) \Delta \mathbf{h}, \tag{101}
\end{aligned}$$

which indicates that the first-order perturbation of the channel gain estimation is

$$\begin{aligned}
\Delta \gamma &= \mathbf{B}^\dagger \Delta \mathbf{h} + \Delta(\mathbf{B}^\dagger) \mathbf{B} \gamma \\
&= \mathbf{B}^\dagger \Delta \mathbf{h} - \mathbf{B}^\dagger \Delta \mathbf{B} \gamma + (\mathbf{B}^H \mathbf{B})^{-1} \Delta \mathbf{B}^H \mathbf{B} \gamma \\
&\quad - (\mathbf{B}^H \mathbf{B})^{-1} \Delta \mathbf{B}^H \mathbf{B} \gamma \\
&= \mathbf{B}^\dagger \Delta \mathbf{h} - \mathbf{B}^\dagger \Delta \mathbf{B} \gamma \\
&= \mathbf{B}^\dagger \Delta \mathbf{h} - \sum_{n=1}^5 \boldsymbol{\Upsilon}_n \mathcal{J}\{\mathbf{V}_n^H \Delta \mathbf{h}\}. \tag{102}
\end{aligned}$$

### D. Proof of Lemma 3

To begin with, we have the first-order approximations of  $\Delta \mathbf{f}_{T,l}$  and  $\Delta \mathbf{f}_{R,l}$  as

$$\Delta \mathbf{f}_{T,l} = \boldsymbol{\Omega}_{T,l} [\Delta \phi_{az}^l, \Delta \phi_{el}^l]^T, \tag{103}$$

$$\Delta \mathbf{f}_{R,l} = \boldsymbol{\Omega}_{R,l} [\Delta \theta_{az}^l, \Delta \theta_{el}^l]^T, \tag{104}$$

respectively, where  $\boldsymbol{\Omega}_{T,l} \in \mathbb{R}^{3 \times 2}$  and  $\boldsymbol{\Omega}_{R,l} \in \mathbb{R}^{3 \times 2}$  are given by

$$\boldsymbol{\Omega}_{T,l} = \begin{bmatrix} -\sin(\phi_{az}^l) \sin(\phi_{el}^l) & \cos(\phi_{az}^l) \cos(\phi_{el}^l) \\ \cos(\phi_{az}^l) \sin(\phi_{el}^l) & \sin(\phi_{az}^l) \cos(\phi_{el}^l) \\ 0 & -\sin(\phi_{el}^l) \end{bmatrix}, \tag{105}$$

$$\boldsymbol{\Omega}_{R,l} = \begin{bmatrix} -\sin(\theta_{az}^l) \sin(\theta_{el}^l) & \cos(\theta_{az}^l) \cos(\theta_{el}^l) \\ \cos(\theta_{az}^l) \sin(\theta_{el}^l) & \sin(\theta_{az}^l) \cos(\theta_{el}^l) \\ 0 & -\sin(\theta_{el}^l) \end{bmatrix}. \tag{106}$$

As a result, the first-order approximations of  $\Delta \boldsymbol{\delta}_l$  and  $\Delta \boldsymbol{\mu}_l$  are obtained as

$$\Delta \boldsymbol{\delta}_l = -c [\tau_l \boldsymbol{\Omega}_{R,l}, \mathbf{f}_{R,l}] [\Delta \theta_{az}^l, \Delta \theta_{el}^l, \Delta \tau_l]^T, \tag{107}$$

$$\begin{aligned}
\Delta \boldsymbol{\mu}_l &= c [\tau_l \boldsymbol{\Omega}_{T,l}, \tau_l \boldsymbol{\Omega}_{R,l}, (\mathbf{f}_{T,l} + \mathbf{f}_{R,l})] \\
&\quad [\Delta \phi_{az}^l, \Delta \phi_{el}^l, \Delta \theta_{az}^l, \Delta \theta_{el}^l, \Delta \tau_l]^T. \tag{108}
\end{aligned}$$

Since  $\mathbf{C}_l = (\mathbf{I} - \boldsymbol{\mu}_l \boldsymbol{\mu}_l^T / \|\boldsymbol{\mu}_l\|^2)$ ,  $\Delta \mathbf{C}_l$  can be given as<sup>5</sup>

$$\begin{aligned}
\Delta \mathbf{C}_l &= 2(\boldsymbol{\mu}_l^T \boldsymbol{\mu}_l)^{-2} (\boldsymbol{\mu}_l^T \Delta \boldsymbol{\mu}_l) \boldsymbol{\mu}_l \boldsymbol{\mu}_l^T \\
&\quad - (\boldsymbol{\mu}_l^T \boldsymbol{\mu}_l)^{-1} (\Delta \boldsymbol{\mu}_l \boldsymbol{\mu}_l^T + \boldsymbol{\mu}_l \Delta \boldsymbol{\mu}_l^T). \tag{109}
\end{aligned}$$

<sup>5</sup>We drop  $\iota_l$  if each path is equality treated.



According to (7), and define  $\mathbf{C} = \sum_{l=1}^L \mathbf{C}_l$ , we have

$$\begin{aligned}
\hat{\mathbf{p}}_{\text{R}} &= \left( \sum_{l=1}^L \mathbf{C}_l + \Delta \mathbf{C}_l \right)^{-1} \sum_{l=1}^L (\mathbf{C}_l + \Delta \mathbf{C}_l) (\boldsymbol{\delta}_l + \Delta \boldsymbol{\delta}_l) \\
&= \left( \mathbf{I} + \sum_{l=1}^L \mathbf{C}^{-1} \Delta \mathbf{C}_l \right)^{-1} \mathbf{C}^{-1} \\
&\quad \sum_{l=1}^L \mathbf{C}_l \boldsymbol{\delta}_l + \Delta \mathbf{C}_l \boldsymbol{\delta}_l + \mathbf{C}_l \Delta \boldsymbol{\delta}_l + \Delta \mathbf{C}_l \Delta \boldsymbol{\delta}_l \\
&\approx \left( \mathbf{I} - \sum_{l=1}^L \mathbf{C}^{-1} \Delta \mathbf{C}_l + \mathbf{C}^{-1} \sum_{l=1}^L \Delta \mathbf{C}_l \mathbf{C}^{-1} \sum_{l=1}^L \Delta \mathbf{C}_l \right) \\
&\quad \mathbf{C}^{-1} \sum_{l=1}^L \mathbf{C}_l \boldsymbol{\delta}_l + \Delta \mathbf{C}_l \boldsymbol{\delta}_l + \mathbf{C}_l \Delta \boldsymbol{\delta}_l + \Delta \mathbf{C}_l \Delta \boldsymbol{\delta}_l \\
&\approx \mathbf{p}_{\text{R}} + \mathbf{C}^{-1} \sum_{l=1}^L \Delta \mathbf{C}_l (\boldsymbol{\delta}_l - \mathbf{p}_{\text{R}}) + \mathbf{C}^{-1} \sum_{l=1}^L \mathbf{C}_l \Delta \boldsymbol{\delta}_l \\
&\quad + \mathbf{C}^{-1} \sum_{l=1}^L \Delta \mathbf{C}_l \Delta \boldsymbol{\delta}_l - \mathbf{C}^{-1} \sum_{l=1}^L \Delta \mathbf{C}_l \mathbf{C}^{-1} \sum_{l=1}^L \mathbf{C}_l \Delta \boldsymbol{\delta}_l \\
&\quad + \mathbf{C}^{-1} \sum_{l=1}^L \Delta \mathbf{C}_l \mathbf{C}^{-1} \sum_{l=1}^L \Delta \mathbf{C}_l (\mathbf{p}_{\text{R}} - \boldsymbol{\delta}_l), \quad (110)
\end{aligned}$$

where higher order approximation is omitted. Therefore, the first-order perturbation of the position estimate, i.e.,  $\Delta \mathbf{p}_{\text{R}} = \hat{\mathbf{p}}_{\text{R}} - \mathbf{p}_{\text{R}}$ , can be obtained as

$$\begin{aligned}
\Delta \mathbf{p}_{\text{R}} &= \mathbf{C}^{-1} \sum_{l=1}^L \Delta \mathbf{C}_l (\boldsymbol{\delta}_l - \mathbf{p}_{\text{R}}) + \mathbf{C}^{-1} \sum_{l=1}^L \mathbf{C}_l \Delta \boldsymbol{\delta}_l \\
&= \mathbf{C}^{-1} \sum_{l=1}^L \check{\mathbf{C}}_l \Delta \boldsymbol{\mu}_l + \mathbf{C}_l \Delta \boldsymbol{\delta}_l, \quad (111)
\end{aligned}$$

where  $\check{\mathbf{C}}_l \in \mathbb{R}^{3 \times 3}$  is given by

$$\begin{aligned}
\check{\mathbf{C}}_l &= \frac{2\boldsymbol{\mu}_l^{\text{T}} (\boldsymbol{\delta}_l - \mathbf{p}_{\text{R}}) \boldsymbol{\mu}_l \boldsymbol{\mu}_l^{\text{T}}}{\|\boldsymbol{\mu}_l\|^4} \\
&\quad - \frac{\boldsymbol{\mu}_l^{\text{T}} (\boldsymbol{\delta}_l - \mathbf{p}_{\text{R}}) \mathbf{I} + \boldsymbol{\mu}_l (\boldsymbol{\delta}_l - \mathbf{p}_{\text{R}})^{\text{T}}}{\|\boldsymbol{\mu}_l\|^2}. \quad (112)
\end{aligned}$$

Substituting the results in (107) and (108) to (111), we arrive at

$$\begin{aligned}
\Delta \mathbf{p}_{\text{R}} &= \sum_{l=1}^L \check{\mathbf{D}}_l [\Delta \theta_{\text{az}}^l, \Delta \theta_{\text{el}}^l, \Delta \tau_l]^{\text{T}} \\
&\quad + \check{\mathbf{E}}_l [\Delta \phi_{\text{az}}^l, \Delta \phi_{\text{el}}^l, \Delta \theta_{\text{az}}^l, \Delta \theta_{\text{el}}^l, \Delta \tau_l]^{\text{T}}, \quad (113)
\end{aligned}$$

where  $\check{\mathbf{D}}_l \in \mathbb{R}^{3 \times 3}$  and  $\check{\mathbf{E}}_l \in \mathbb{R}^{3 \times 5}$

$$\check{\mathbf{D}}_l = -c \left( \sum_{\ell=1}^L \mathbf{C}_\ell \right)^{-1} \mathbf{C}_l [\tau_l \boldsymbol{\Omega}_{\text{R},l}, \mathbf{f}_{\text{R},l}], \quad (114)$$

$$\check{\mathbf{E}}_l = c \left( \sum_{\ell=1}^L \mathbf{C}_\ell \right)^{-1} \check{\mathbf{C}}_l [\tau_l \boldsymbol{\Omega}_{\text{T},l}, \tau_l \boldsymbol{\Omega}_{\text{R},l}, (\mathbf{f}_{\text{T},l} + \mathbf{f}_{\text{R},l})]. \quad (115)$$

With the results in Lemma 2, we derive the results in (59).